MULTIPLE EQUILIBRIA AND THEIR STABILITY IN A BAROTROPIC AND BAROCLINIC ATMOSPHERE

by

SANDRO RAMBALDI

Laurea in Fisica, University of Bologna

(1974)

SUBMITTED TO THE DEPARTMENT OF
METEOROLOGY AND PHYSICAL OCEANOGRAPHY
IN PARTIAL FULFILLMENT OF THE
REQUIREMENTS FOR THE DEGREE OF

DOCTOR OF PHILOSOPHY

at the

MASSACHUSETTS INSTITUTE OF TECHNOLOGY

August 1982

Signature of Author _____
Department of Meteorology and Physical Oceanography
August, 1982

Certified by _____
Glenn R. Flierl
Thesis Supervisor

Accepted by: _____
Ronald G. Prinn
Chairman, Departmental Graduate Committee

MULTIPLE EQUILIBRIA AND THEIR STABILITY IN A BAROTROPIC AND BAROCLINIC ATMOSPHERE

by

SANDRO RAMBALDI

Submitted to the Department of Meteorology and Physical Oceanography in August 1982 in partial fulfillment of the requirements for the Degree of Doctor of Philosophy

ABSTRACT

This work is divided into three independent sections; the common subject is the role of topography in the forcing of stationary waves.

In the first section we study the multiple equilibria problem in a barotropic atmosphere and we examine the form-drag instability in a simple model, considering in some detail the processes involved. We study how the system approaches the equilibria (stable case) or departs from them (unstable case). Then we consider the non-linear problem discussing the properties of the solution using the conservation of energy and potential enstrophy and introducing a potential function for the zonal flow. The limit for small dissipation and forcing is then discussed and compared with numerical solutions.

In the second section we examine a two-layer highly truncated channel model with topography to study multiple equilibria and to discuss their stability. We find that all the Charney-Straus multiple equilibria require meridional temperature gradients which are highly baroclinically unstable. After a detailed study we demonstrate that the flux of angular momentum from tropical latitudes is able to produce one equilibrium which is baroclinically stable (in the two layer model). For low values of the external radiation heating the stationary topographically forced wave alone satisfies all

the balances, while for larger values of the external radiation forcing the stationary topographically forced wave collaborates with shorter, more baroclinically unstable, moving, synoptic scale waves.

In the third and last section we have presented some simple but general theorems on the upward transport of zonal momentum and energy by stationary quasi-geostrophic waves and by the mean meridional circulation induced by these waves.

Thesis Supervisor : Dr. Glenn R. Flierl

Title : Associate Professor of Oceanography

Acknowledgments

This work began and was almost completed under the guidance of the late Prof. Jule G. Charney. His constructive criticisms and helpful comments deepened my understanding of my particular problem and its relation to more general ones.

Throughout all my studies Profs. Glenn Flierl, Peter Stone and Ray Pierrehumbert were ready sources for advice and consultation.

During 1982 Prof. Glenn Flierl became my advisor and supported my efforts. He was always available for discussion, providing useful alternative viewpoints.

The manuscript was carefully corrected by Joel Sloman and the figures were skillfully and promptly drawn by Ms. Isabelle Kole. The research was supported by the National Science Foundation under grant NSF 76-20070ATM.

Table of contents

SECTION 3

STATIONARY ADIABATIC FRICTIONLESS FLOW OVER TOPOGRAPHY

SECTION 1

FORM-DRAG INSTABILITY AND MULTIPLE EQUILIBRIA IN THE BAROTROPIC CASE

1. Introduction

In 1979, Charney and his coauthors wrote a series of papers which first developed the idea that the atmosphere may have several possible equilibria states for the same external forcing. In the simplest problem, barotropic flow in a beta plane channel with topography, forced by a momentum source, Charney and Devore (1979) demonstrated that the non linear equations arising from a low order spectral truncation did have multiple stable states. Given the forcing, within certain parameter ranges, two possible equilibria were found, one with a weak zonal flow and strong waves and one with strong zonal flow and weak waves. A higher resolution numerical code was used to assess the degree to which their truncated model rapresented solutions of the original problem.

In further work, Charney and Straus (1980), examined the effects of baroclinicity, Charney, Shukla and Mo (1981),

applied the model to earth's topography; finally the work of Reinhold (1981), suggests possible directions in which the principles of multiple equilibria might be modified when synoptic scale instabilities occur in addition to weak topographic forcing of the long waves.

Our purpose here, however, is to examine the simplest model with form-drag instability and multiple equilibria: a model similar to that of Hart (1979) or Charney and Flierl (1980). We shall consider the processes involved in form drag instability in some detail in order to explicate the mechanism in the most straightforward barotropic case.

As new physical contributions we point out how the form drag is felt by the zonal flow through the ageostrophic component of the flow and in paragraph 3 and 5 we describe the mechanism and the properties of the form-drag instability emphasizing the study of the quantities that can be measured. In paragraph 6 we discuss the form-drag instability as a simple consequence of the simultaneous conservation of energy and potential enstrophy. In the viscous case some numerical calculations have been done to show how the system approaches the stable equilibria.

As technical contribution we have introduced a new potential function; in this way we have three degree of freedom and three conserved quantities and we are able to

give a simple but complete qualitative discussion of the properties of our system in the inviscid case.

2. Equations of motion

The simplest set of equations which illustrate the form drag instability and multiple equilibria are those of Hart (1979) describing the coupled evolution of the x-independent flow and the topographically forced waves. We derive similar equations without using any asymptotic expansion. This new derivation clearly points out the importance of the ageostrophic components in the interaction between the waves and the zonal flow. The potential vorticity equation for wave flows over y-independent topography is

$$\frac{\partial}{\partial t}\frac{\partial^2\psi}{\partial x^2} + U\frac{\partial}{\partial x}\left(\frac{\partial^2\psi}{\partial x^2} + f_o\frac{h}{H}\right) + \beta\frac{\partial\psi}{\partial x} + \frac{1}{\tau}\frac{\partial^2\psi}{\partial x^2} = 0 \qquad (2.1)$$

where ψ is the geostrophic streamfunction

U is the eastward component of the geostrophic wind

V is the northward component of the geostrophic wind

f_o is the Coriolis parameter at mid-latitude

β is derivative of the Coriolis parameter = (df /dy)

h is the height of the topography

H is the depht of the fluid

and τ is the dissipation time scale (due to friction in upper and lower Ekman layers). The evolution of the mean zonal wind U cames from the x-averaged momentum equation where periodicity has been assumed

$$\frac{\partial U}{\partial t} = f_0 \overline{v'} - \frac{\partial}{\partial y}(\overline{uv}) - \frac{1}{\tau}\left(U - \frac{1}{\tau}U^*\right) \qquad (2.2)$$

When the topography is y-independent the Reynolds' stresses disappear and the changes in the zonal flow are due to dissipation, external forcing, U^*, and to the ageostrophic part of the y-component of the velocity $\overline{v'}$. This ageostrophic part of the velocity can be directly related to the form drag as follows: we calculate the mean meridional flux of mass here, denoted by M

$$M = \overline{(H-h)v} = H\overline{v'} - \overline{hv} - \overline{hv'} \qquad (2.3)$$

The form drag is given by

$$-\frac{1}{L_x}\int_0^{L_x} P\cos\theta\, ds = -\frac{1}{L_x}\int_0^{L_x} P\frac{\partial h}{\partial x}\, dx \simeq -\rho_0 f_0 \overline{\psi\frac{\partial h}{\partial x}} \qquad (2.4)$$

where P is the atmospheric ground pressure and θ is the angle from horizontal to the inward normal to the surface. To lower order the meridional mass flux simplifies to

$$M = -\overline{hv} + H\overline{v'} = \overline{\psi \frac{\partial h}{\partial x}} + H\overline{v'} \qquad (2.5)$$

where the first term represent the geostrophic contribution to the form drag.

In a y-independent problem, the mean meridional mass flux could still depend on time but the simplest case is that of no net flux

$$M = 0 \quad \rightarrow \quad \overline{v'} = -\frac{1}{H}\overline{\psi \frac{\partial h}{\partial x}} \qquad (2.6)$$

(which can be justified if the flow is assumed to be confined in a very wide channel). With these assumptions, our system of equations becames

$$\frac{\partial}{\partial t}\frac{\partial^2 \psi}{\partial x^2} + U\frac{\partial}{\partial x}\left(\frac{\partial^2 \psi}{\partial x^2} + f_0 \frac{h}{H}\right) + \beta \frac{\partial \psi}{\partial x} + \frac{1}{\tau}\frac{\partial^2 \psi}{\partial x^2} = 0 \qquad (2.7)$$

$$\frac{\partial U}{\partial t} = -\frac{f_0}{H}\overline{\psi \frac{\partial h}{\partial x}} - \frac{1}{\tau}\left(U - \frac{1}{2}U^*\right) \qquad (2.8)$$

The solution of the system (2.7) and (2.8) can be found with a Fourier decomposition of topography and streamfunction

$$h = \Sigma_\mu h_\mu \sin(k_\mu x + \varphi_\mu)$$

$$\Psi = - Uy + \Sigma_\mu A_\mu \sin(k_\mu x + \varphi_\mu) + B_\mu \cos(k_\mu x + \varphi_\mu)$$

Equations (2.7) and (2.8) became

$$\dot{U} = - \frac{1}{2} \frac{f_o}{H} \Sigma_\mu k_\mu h_\mu B_\mu - \frac{1}{\tau} \left(U - \frac{1}{2} U^* \right) \qquad (2.9)$$

$$\dot{A}_\mu = k_\mu \left(U - \beta / k_\mu^2 \right) B_\mu - \frac{1}{\tau} A_\mu \qquad (2.10)$$

$$\dot{B}_\mu = - k_\mu \left(U - \beta / k_\mu^2 \right) B_\mu + f_o k_\mu \frac{h_\mu}{H} U - \frac{1}{\tau} B_\mu \qquad (2.11)$$

3. Form-drag instability

The simplest system containing the form drag interaction can be obtained with a single mode topography

$$h = \bar{h} \sin k x \tag{3.1}$$

Under this assumption our system of equations can be divided into a set of sub-systems; for $k_\mu \neq k$ we get

$$\dot{A}_\mu = k_\mu \left(U - \beta / k_\mu^2\right) B_\mu - \frac{1}{\tau} A_\mu \tag{3.2}$$

$$\dot{B}_\mu = - k_\mu \left(U - \beta / k_\mu^2\right) B_\mu - \frac{1}{\tau} B_\mu \tag{3.3}$$

Even if U is time dependent we can see from the energy equation

$$\frac{d}{dt}\left(A_\mu^2 + B_\mu^2\right) = - \frac{2}{\tau}\left(A_\mu^2 + B_\mu^2\right) \tag{3.4}$$

that these modes simply dissipate. The system (3.2) and (3.3) can be solved exactly; introducing a complex notation the solution is given by:

$$A_\mu(t)+iB_\mu(t) = \left[A_\mu(0)+iB_\mu(0)\right] e^{-\frac{t}{\tau}} e^{-i\int_0^t \left[U(t')-\beta/k_\mu^2\right] dt'} \qquad (3.5)$$

This is just a decaying travelling Rossby wave. To determine the time dependence of the zonal flow and to study the role of the topography we must consider the case $k_\mu = k$; we then have the following system

$$\dot{U} = -\frac{1}{2} f_0 k \frac{\bar{h}}{H} B - \frac{1}{\tau}\left(U - \frac{1}{2}U^*\right) \qquad (3.6)$$

$$\dot{A} = k\left(U-\beta/k^2\right)B - \frac{1}{\tau}A \qquad (3.7)$$

$$\dot{B} = -k\left(U-\beta/k^2\right)A + f_0 k \frac{\bar{h}}{H} U - \frac{1}{\tau}B \qquad (3.8)$$

To clarify the role of the different parameters involved let us introduce non-dimensional variables as follows:

$$\begin{aligned} t &= (k/\beta)\, t' \\ U &= (\beta/k^2)\cdot U' \\ (A, B) &= (\beta/k^3)\ (A', B') \\ \bar{h} &= H h' \end{aligned} \qquad (3.9)$$

With these substitutions we get two non-dimensional parameters

$$\lambda = h' k f_0 / \beta \simeq h' k a \qquad (3.10)$$

that describes the importance of the mountain and

$$\nu = \frac{k}{\beta \cdot \tau} \simeq \frac{k \cdot a}{f_0 \tau} \qquad (3.11)$$

which describes the dissipative effects. Introducing the zonal wave number n , $k = n*(2\pi/2\pi a \cos \varphi)$, where a is the earth radius and φ is a middle latitude, here chosen to be 45°, and the following typical atmospheric numbers, $h' \sim .2$, $f_0 \simeq 10^{-4}$ sec^{-1} , $\tau \sim$ 10 days $\sim 8.6*10^5$ sec, we get the following values:

$$\lambda \simeq .28\mu \qquad \nu \simeq .016\mu$$

With these non-dimensional parameters our system of equations, (3.6)-(3.7)-(3.8), dropping the primes, becomes

$$\dot{U} = -\frac{1}{2}\lambda B - \nu (U - \frac{1}{2} U^*) \qquad (3.12)$$

$$\dot{A} = (U-1)B - \nu A \qquad (3.13)$$

$$\dot{B} = -(U-1)A + \lambda U - \nu B \qquad (3.14)$$

* The mechanism of form-drag instability can be seen quite clearly from these equations and figures 1 and 2. Let us neglect forcing and dissipation and consider first the situation when U is less than the resonant speed $U<1$, or $U < \beta/k^2$ in dimensional quantities.

The wave generated by the flow has vorticity which is in phase with the topography since the flow is dominantly constrained to follow the geostrophic contours, south on upslopes and north on downslopes, corresponding to cyclonic curvature over the peaks. In this inviscid steady-state situation there is no form drag, an illustration of wave-mean flow non interaction in the absence of time dependence or friction (Pedlosky, private comunication).

If we perturb this flow by introducing vorticity which is 90° out of phase with the topography, the flow will evolve in time. There are two different tendencies for the flow: an acceleration or deceleration of the mean flow and a change in the vorticity distribution.

If the initial vorticity perturbation lags the topography by 90° (figure 1.b), corresponding to $B > 0$, the

* This discussion of form-drag instability was contributed by Prof. Glenn R. Flierl

pressure disturbance will lead the topography so that the form drag will decelerate the mean flow (figure 1.c). Changes in vorticity are induced by westward Rossby wave propagation and eastward advection by the mean flow. For subresonant mean flow, the westward wave propagation tendency is larger than the eastward mean flow so that the vorticity begins to increase over the crest (figure 1.d).

From the first derivative patterns, we can explore the second time derivative of the vorticity, ζ_{tt}, to see whether the initial perturbation is reinforced or counteracted. There are three different mechanisms for generating ζ_{tt}: wave propagation and mean advection of the ζ_t field, topographic generation by the U_t field and additional advection of the basic state vorticity field by the U_t flow. The wave propagation plus mean advection continues to lie toward the west, leading to a ζ_{tt} of opposite sign from the original perturbation (figure 1.e). The decrease in the flow over topography leads to a decrease in vorticity in the troughs, a ζ_{tt} which leads the topography by 90°. Finally, the advection of the basic vorticity (the term which would correspond to $-\dot{U}A$ in the differentiated form of Eq. (3.14)) also leads the topography since $\dot{U}$ is negative, and the basic vorticity is correlated with h. For $U < 1$, then, all of the contributions to ζ_{tt} are of opposite sign to the initial

perturbation so that the topographic wave is neutrally stable.

When $U > 1$, however, the situation is quite different (figure 2). The basic equilibrium distribution of vorticity is anti-correlated with the topography since the changes in relative vorticity rather than planetary vorticity tend to balance the vortex stretching over the topography. If we introduce the same form of perturbation, we still get a form drag retarding the mean flow but the wave propagation tendency now has a reversed sign. The perturbation advects downstream faster than it propagates westward. As we look at the changes in the ψ_{tt} term, however, the doppler-shifted wave propagation still generates a flow leading the topography (figure 2.c). The tendency from the decrease in the mean flow over the topography is also the same as before (figure 2.f). But the third contribution now has the opposite sign since the original equilibrium vorticity is now of opposite sign from the topography (figure 2.g). Thus there is the possibility when the equilibrium state vorticity is sufficiently large (which occurs near resonance) that this term will dominate the other two and ψ_{tt} will reinforce the original perturbation, leading to an instability of the flow. The basic mechanism for form drag instability, therefore, can be summarized as follows: when the zonal flow is

supercritical, the vorticity is anticorrelated with the topography. Decreases in the zonal flow result in this anti-correlated vorticity shifting westward leading to pressure patterns which have highs on the upslopes and lows on the downslopes. This in turn leads to a form drag which decelerates the zonal flow further.

4. Non-linear behaviour for the inviscid case

As we have seen ε is a small parameter and we can solve our system by developing all our unknowns in a power series of ε :

$$(U, A, B) = (U_0, A_0, B_0) + \varepsilon (U_1, A_1, B_1) + O(\varepsilon^2)$$

We shall study the non-linear behaviour only of the zero-order equations which are:

$$\dot{U}_0 = -\frac{1}{2} \lambda B_0 \qquad (4.1)$$

$$\dot{A}_0 = (U_0 - 1) B_0 \qquad (4.2)$$

$$\dot{B}_0 = -(U_0 - 1) A_0 + \lambda U_0 \qquad (4.3)$$

This inviscid problem has two independent conserved quantities

$$E_0 = U_0^2 + \frac{1}{2} (A_0^2 + B_0^2) \qquad (4.4)$$

$$Q_0 = (U_0 - 1)^2 + \lambda A_0 \qquad (4.5)$$

As Charney and DeVore pointed out, the first quantity represents the total energy and the second quantity a combination of the total energy with the potential enstrophy. The existence of these two integrals of motion allows a complete analytical solution of the system (4.1)-(4.2)-(4.3) in terms of elliptic functions.

As we shall see a full discussion of the properties of the solutions of this system can be done without solving explicitly. As first step we derive a simple second order equation only in U; we substitute the definition of Q in Eq. (4.3) getting

$$\dot{B}_o = \frac{1}{\lambda}(U_o - 1)\left[(U_o-1)^2 - Q_o\right] + \lambda U_o \qquad (4.6)$$

After a time derivative of (4.1) and the substitution of B_o from (4.6) we get:

$$\ddot{U}_o = -\frac{1}{2}(U_o - 1)\left[(U_o-1)^2 - Q_o\right] - \frac{1}{2}\lambda^2 U_o \qquad (4.7)$$

It is useful at this point to introduce a more explicit expression for Q_o as function of the stationary solutions.

If U has any chosen value $\bar{U}$, the system

(4.1)-(4.2)-(4.3) gives a stationary forced wave with amplitude

$$\bar{B} = 0 \tag{4.8}$$

$$\bar{A} = \frac{\lambda \bar{U}}{\bar{U} - 1} \tag{4.9}$$

On figure 3, the light lines represent lines of constant Q_o, Eq. (4.5), while the heavy line represents the stationary solutions, from here on called the equilibria curve, Eq. (4.9). At least one intersection on the branch number one always exists; therefore the conserved quantity Q can always be written as a function of the coordinates of this intersection, here denoted with ($\bar{U}$, $\bar{A}$, $\bar{B}$), as follows

$$Q_o = (\bar{U} - 1)^2 + \lambda^2 \frac{\bar{U}}{\bar{U} - 1} \tag{4.10}$$

Using this definition and defining

$u = U_o - \bar{U}$ "distance" from the equilibrium

$\Delta = 1 - \bar{U}$ "distance of the equilibrium from the resonance"

Eq. (4.7) can be rewritten as

$$2\ddot{u} = -\frac{1}{\Delta}\left(\lambda^2+2\Delta^3\right)u + 3\Delta u^2 - u^3 \qquad (4.11)$$

or multiplying both sides by $\dot{u}$

$$\frac{d}{dt}\left[\dot{u}^2 + V(u)\right] = 0 \qquad (4.12)$$

where $V(u)$ is a potential function defined by

$$V(u) = \frac{1}{2\Delta}\left(\lambda^2+2\Delta^3\right)u^2 - \Delta u^3 + \frac{1}{4}u^4 \qquad (4.13)$$

We have a mathematical analogy between the time evolution of the zonal wind and the motion of a particle moving in a one-dimensional space with a potential energy given by $\frac{1}{2}V(u)$.

With this potential we can discuss the general behaviour of our solutions: in particular we can see that the linear stability properties of the points of equilibrium are governed by the sign of $\left(\lambda^2+2\Delta^3\right)/\Delta$, in agreement with the linear analysis of Charney and DeVore; the non linear behaviour is dominated by the positive sign of the fourth

order term and we have a non linear stability for all the points of equilibrium.

Depending on the number of points of equilibrium our system behaves in different ways; for a given Q_o, or Δ, the points of equilibrium are given by $\ddot{u} = 0$ or $\frac{dV}{du} = 0$, i.e.

$$\frac{1}{\Delta} u \left(\Delta u^2 - 3\Delta^2 u + \lambda^2 + 2\Delta^3 \right) = 0 \qquad (4.14)$$

the root $u_1 = 0$ represents the equilibrium point, ($\overline{U_1}$, $\overline{A_1}$, $\overline{B_1}$), previously discussed while the other two roots

$$u_{2,3} = \frac{1}{2} \Delta \left(3 \mp \sqrt{1 - 4\lambda^2/\Delta^3} \right) \qquad (4.15)$$

represent the other intersections of the constant Q_o line with the equilibria curve. The point $P_1 = (\overline{U_1}, \overline{A_1}, \overline{B_1})$ will be the only equilibrium if

$$\Delta^3 < 4\lambda^2 \qquad (4.16)$$

In this case the potential function, Eq. (4.13), has only one

minimum and the system oscillates periodically around $(\bar{U}_1, \bar{A}_1, \bar{B}_1)$.

For $\Delta^3 > 4\lambda$ three intersections are present; from the expression for the potential function, (4.13), it is evident that the second equilibrium point is an unstable point while the other two are stable. Some straight-forward analysis shows that the minimum on the branch 1 is always lower than the one on the branch 2. In figure 4 we have drawn the potential function for this case. The motion is always periodic; if we start close to the equilibria it consists of a simple oscillation while if we start far from the equilibria the system oscillates from one attractor basin to the other.

5. Approach to the equilibria in the viscous case

Until now we have considered the non-dissipative case; in presence of a small dissipation and forcing the evolution of our system is essentially similar except that now we no longer have an equilibrium curve but only one or three equilibria and from any points of our phase-space the system goes towards the stable points while approximately conserving the potential enstrophy and the energy. To get a better understanding of the way in which the system approaches the stable equilibria we can study the behaviour of small perturbations around these stable equilibria. From Eqs. (3.12)-(3.13)-(3.14) we find that these equilibria are defined by:

$$\overline{B} = -\frac{2\nu}{\lambda}\left(\overline{U} - \frac{1}{2}U^*\right) \tag{5.1}$$

$$\overline{B} = \nu\,\frac{\overline{A}}{\overline{U}-1} \tag{5.2}$$

$$\overline{A} = \lambda\,\frac{\overline{U}}{\overline{U}-1} + O(\nu^2) \tag{5.3}$$

It is convenient to get an expansion of the coordinates of the equilibrium point in powers of ν; for $\lambda^2 \neq (U_0-1)(4U_0+2-U^*)$ we have:

$$\bar{A} = A_0 + O(\nu^2) \tag{5.4}$$

$$\bar{B} = \nu \frac{A_0}{A_0 - 1} + O(\nu^2) \tag{5.5}$$

$$\bar{U} = U_0 + O(\nu^2) \tag{5.6}$$

where A_0 and U_0 are related by:

$$A_0 = \lambda \frac{U_0}{U_0 - 1} \tag{5.7}$$

This is a zero order relation and implies that the equilibria point must be on the inviscid equilibria curve.

Secondly, we have

$$A_0 = -\frac{1}{\lambda}(2U_0 - U^*)(U_0 - 1) \tag{5.8}$$

which comes from the first order equations and implies the balance between the generation and the dissipation.

A graphical solution of this system is shown in figure 5 for different values of the external forcing U^*. The heavy line represents the equilibria curve (5.7), while the light curve rapresents points where the generation is in balance with the dissipation, Eq. (5.8), in the plane (U, A). As we can see for small forcing we have only one

stable equilibrium and for larger values of the forcing we can get three equilibria with the one in the middle unstable.

Denoting, as before, with (u,a,b) the perturbations from ($\bar{U}$,$\bar{A}$,$\bar{B}$) we get the following equations:

$$\dot{u} = -\frac{1}{2}\lambda b - \nu u \tag{5.9}$$

$$\dot{a} = (\bar{U}-1)b + \bar{B}u - \nu a \tag{5.10}$$

$$\dot{b} = -(\bar{U}-1)a + (\lambda-\bar{A})u - \nu b \tag{5.11}$$

Having a system with constant coefficients, we can look for a solution in the form $(u,a,b)*e^{\sigma t}$ and we get the following eigenvalue problem:

$$(\sigma+\nu)^3 + \omega^2(\sigma+\nu) - \frac{1}{2}\nu\lambda\bar{A} = 0 \tag{5.12}$$

where

$$\omega^2 = (\bar{U}-1)^2 + \frac{1}{2}\lambda(\lambda-\bar{A}) \tag{5.13}$$

expanding the eigenvalues in power of ν

$$\sigma = \sigma_0' + \nu \sigma_1' + O(\nu^2)$$

$$\omega = \omega_0 + O(\nu^2)$$

we get

$$\sigma_0' (\sigma_0'^2 + \omega_0^2) = 0 \qquad (5.14)$$

$$\sigma_1' = -1 + \frac{1}{2} \frac{A_0}{\omega_0^2 + 3\sigma_0^2} \qquad (5.15)$$

We have three solutions: one real

$$\sigma_1 = -\nu \left(1 - \frac{1}{2} \frac{\lambda A_0}{\omega_0^2}\right) + O(\nu^2) \qquad (5.16)$$

and two complex coniugates

$$\sigma_{2,3} = \pm i\omega_0 - \nu \left(1 + \frac{1}{4} \frac{\lambda A_0}{\omega_0^2}\right) + O(\nu^2) \qquad (5.17)$$

The first eigenvalue has for its eigenvector

$$b = 0 \qquad a = -\frac{\lambda}{(U_0 - 1)^2} u \qquad (5.18)$$

corresponding to the direction tangent to the equilibria curve in the plane B = 0 of figure 3. The other two eigenvalues have an oscillatory part with a much shorter time scale and therefore, on the average, the solution

approaches the point of equilibrium moving along the "equilibria curve" with a damped motion.

These two complex eigenvalues with their eigenvectors

$$\frac{b}{\sigma_{2,3}} = -\frac{2}{\lambda} u = \frac{1}{\bar{U}-1} a \qquad (5.19)$$

give rise to a damped oscillation in the zonal flow together with damped standing and propagating waves. In fact the stream-function for the wavy part of these perturbations can be written as:

$$\psi = A \cdot Z(x,t)\, e^{-\nu\left(1+\frac{1}{4}\frac{\lambda A_0}{\omega_0^2}\right)t} \qquad (5.20)$$

where

$$Z(x,t) = \sin kx \cos\omega_0 t - \frac{\omega_0}{\bar{U}-1} \cos kx \sin\omega_0 t$$

$$\omega_0^2 = (\bar{U}-1)^2 - \frac{1}{2}\frac{\lambda^2}{\bar{U}-1} > 0$$

We have two cases: for the super-resonant case, $\bar{U} > 1$, we have $\omega_0^2 < (\bar{U}-1)^2$ and

$$Z(x,t) = \sin(kx-\omega_0 t) + \left(1 - \frac{\omega_0}{\bar{U}-1}\right) \cos kx \sin\omega_0 t$$

where the first term rapresents an eastward moving "slow Rossby wave" and the second term a smaller standing wave out of phase with the topography; for the sub resonant-case, $\bar{U} < 1$, we have $\omega_o^2 > (\bar{U}-1)^2$ and

$$Z(x,t) = \frac{\omega_o}{1-\bar{U}} \left[\sin(kx+\omega_o t) - \left(1 - \frac{1-\bar{U}}{\omega_o}\right) \sin kx \cos \omega_o t \right.$$

where the first term represents a westward moving "fast Rossby wave" and the second term a smaller standing wave in phase with the topography.

6. Stability of the equilibria

Using figures 6.(a) and 6.(b) we can discuss the properties of the equilibria; for a chosen Q , dotted parabola in figure 6.(a), we have three intersections with the equilibria curve, heavy line; for each intersection we have drawn the energy ellipsoid, dashed lines, Eq. (4.4). As we can see, for the two stable equilibria C and E, any nearby point, on the Q_o curve, has larger energy and cannot be reached. For the unstable equilibrium D, the energy ellipsoid intersects the Q surface so that neighboring points with finite B's and smaller energies in the U and A fields can be reached conserving energy and potential enstrophy; this trajectory is the heavy dashed line of figure 6.(b).

7. Numerical integration

To illustrate part of the linear and non linear dynamics of the preceeding discussions we have integrated, with a fourth order Runge Kutta method, the system (3.12)-(3.13)-(3.14). We have chosen the following values λ = .8 and ν = .05 . In figures 7a,7b,7c we have considered, for different initial conditions, the system with three equilibria (C,D,E); as we can see, the two

stable equilibria (C,E) are approached with oscillations almost on the isolines of Q, together with a net displacement along the inviscid equilibria curve toward the stable equilibrium.

In figure 8 we have considered parameters such that the system has only one equilibrium. We no longer have any forced and damped equilibria on the branch number two of the equilibrium curve, but the equilibrium curve is still a zero order equilibrium solution so that we can see damped oscillations, with Q nearly conserved, together with a mean motion along the equilibrium curve toward the saddle point. After crossing this point, the oscillations grow again and the system evolves toward the only equilibrium left.

REFERENCES

Charney, J.G., J.G. DeVore, 1979: Multiple flow equilibria in the atmosphere and blocking. J. Atmos. Sci., 36, 1205-1216.

Charney, J.G. and D.M. Strauss, 1980: Form-drag instability, multiple equilibria and propagating planetary waves in baroclinic, orographically forced, planetary wave systems. J. Atmos. Sci., 37, 1157-1176

Charney, J.G., J. Shukla and K.C. Mo, 1981: Comparison of a barotropic blocking theory with observation. J. Atmos. Sci. 38,

Charney, J.G. and G.R. Flierl, 1980: Oceanic analogues of large-scale atmospheric motions. Evolution of physical oceanography. Edited by B.A. Warren and C.Wunsch M.I.T. Press. 504-548

Hart, J.E., 1979: Barotropic quasi-geostrophic flow over anisotropic mountains. J. Atmos. Sci., 36, 1736-1746

Reinhold, B.B., 1981: Dynamics of weather regimes: quasi stationary waves and blocking. Ph.D. Thesis, M.I.T., Cambridge, Mass. 02139.

FIGURE CAPTIONS

Figure 1 : see text

Figure 2 : see text

Figure 3 : The heavy line represents the equilibrium curve, and the light lines are contours of constant Q in the plane (U, A).

Figure 4 : Shape of the potential function for different value of .

Figure 5 : Graphical solution of Eq. (1.48), heavy line, for different values of the forcings U , Eq. (1.49).

Figure 6 : The equilibria points (C, D, E) are points in which the energy and the potential enstrophy surfaces are tangent and the stability is determined by whether nearby points can be reached.

Figure 7 : Examples of time evolutions, starting from different regions of the phase space in presence of three equilibria (C, D, E). The heavy line represents the trajectory of the system, the medium heavy line represents the equilibria curve and the light lines are the intersections of the constant Q surfaces with the (U, A) plane. For this evolution we have chosen: U = 4.8, γ = .05 and λ = .8 .

Figure 8 : As in figure 7 but in presence of only one equilibrium, C. For this evolution we have chosen: U = 4.8, γ = .05 and λ = .8 .

($U < \beta/k^2$ CASE)

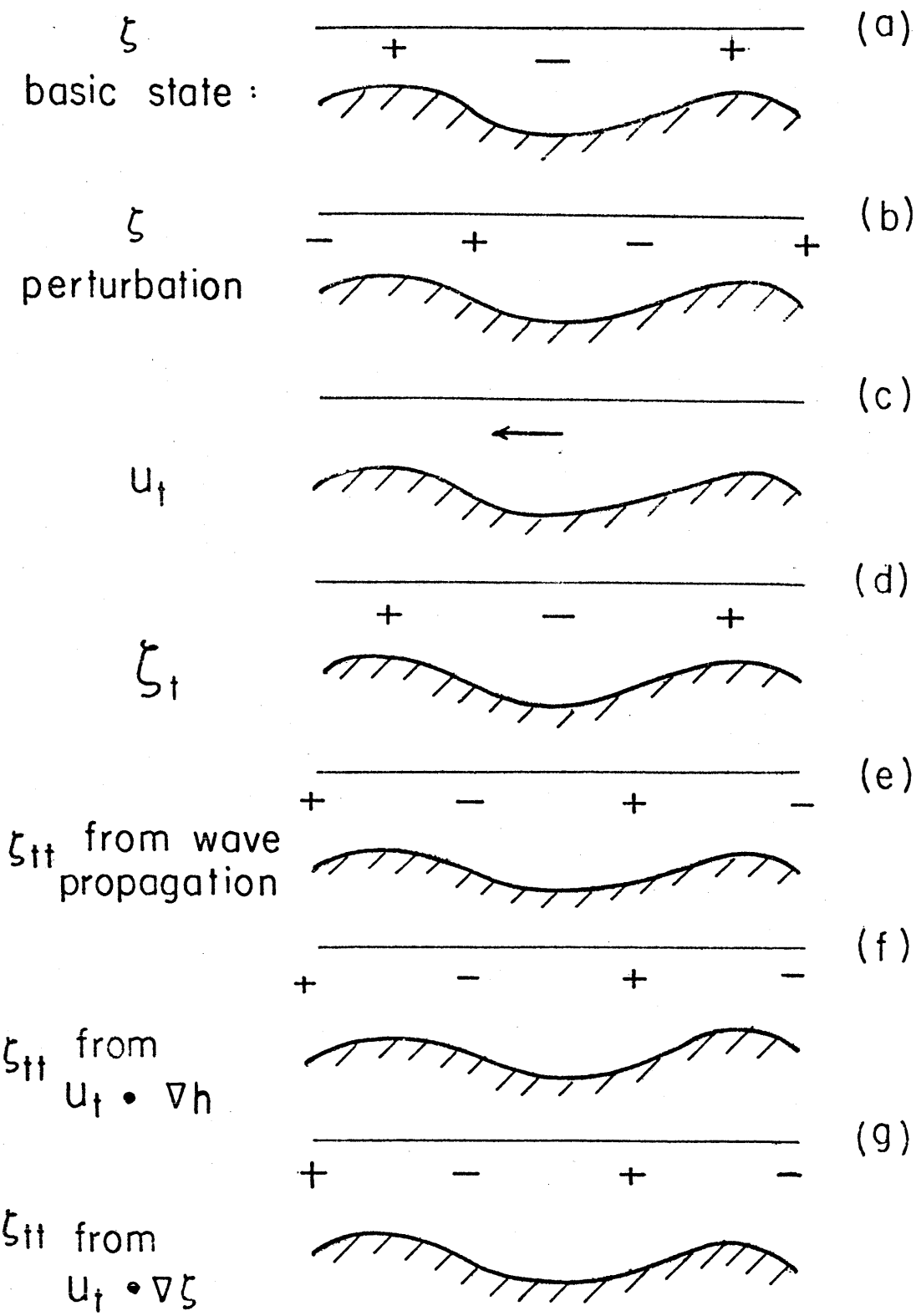

($U > \beta / k^2$ CASE)

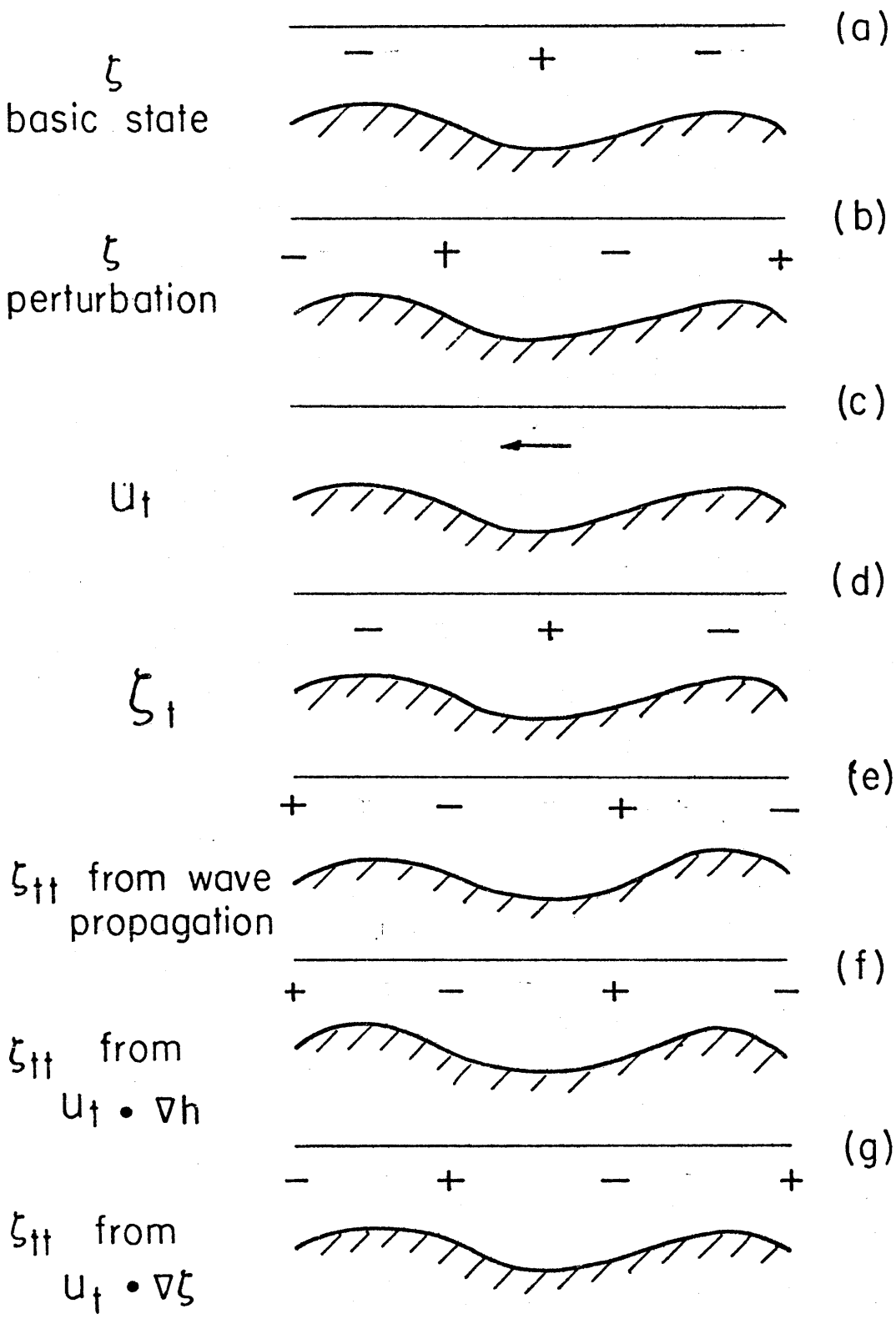

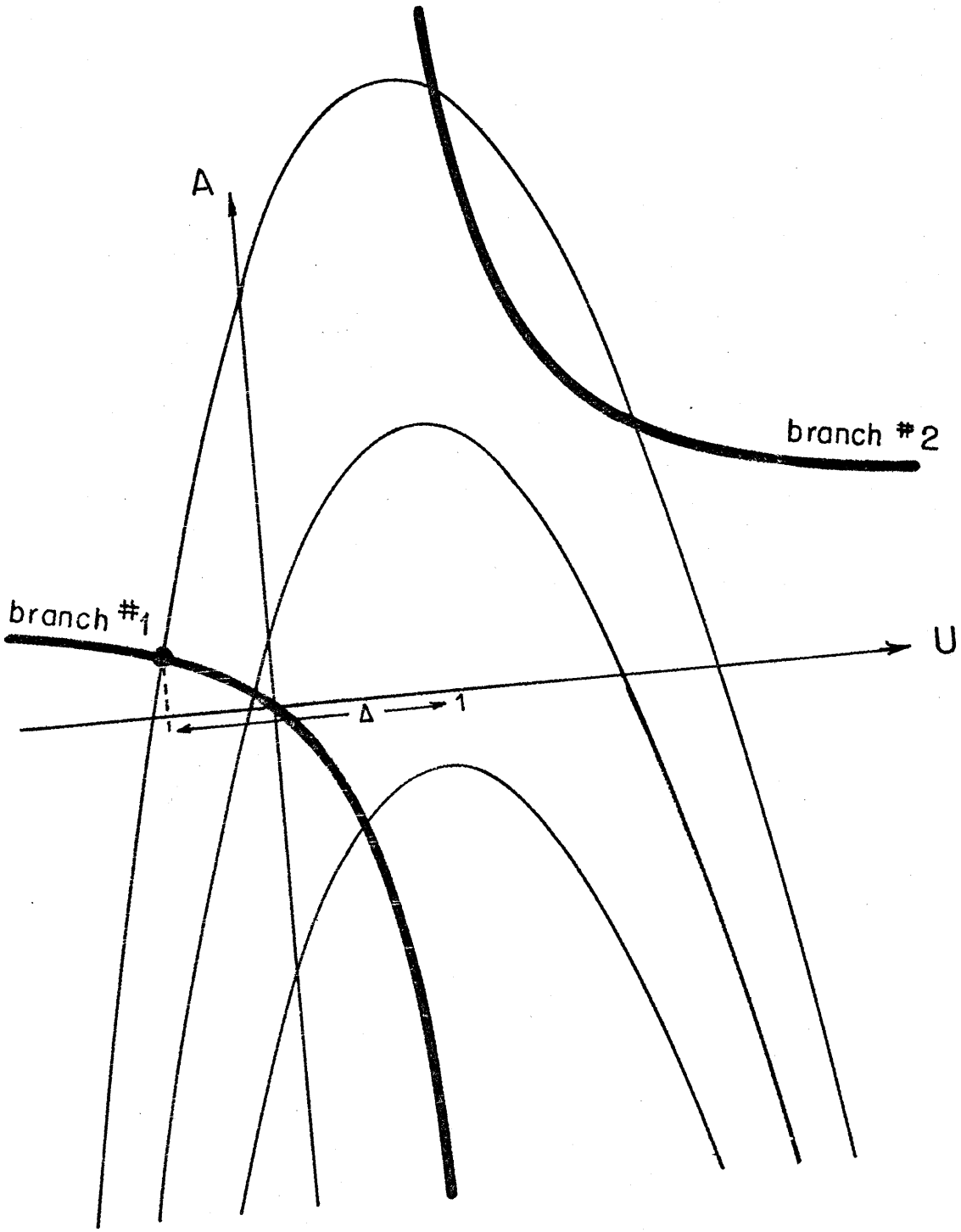
A
branch #2
branch #1
U
Δ → 1

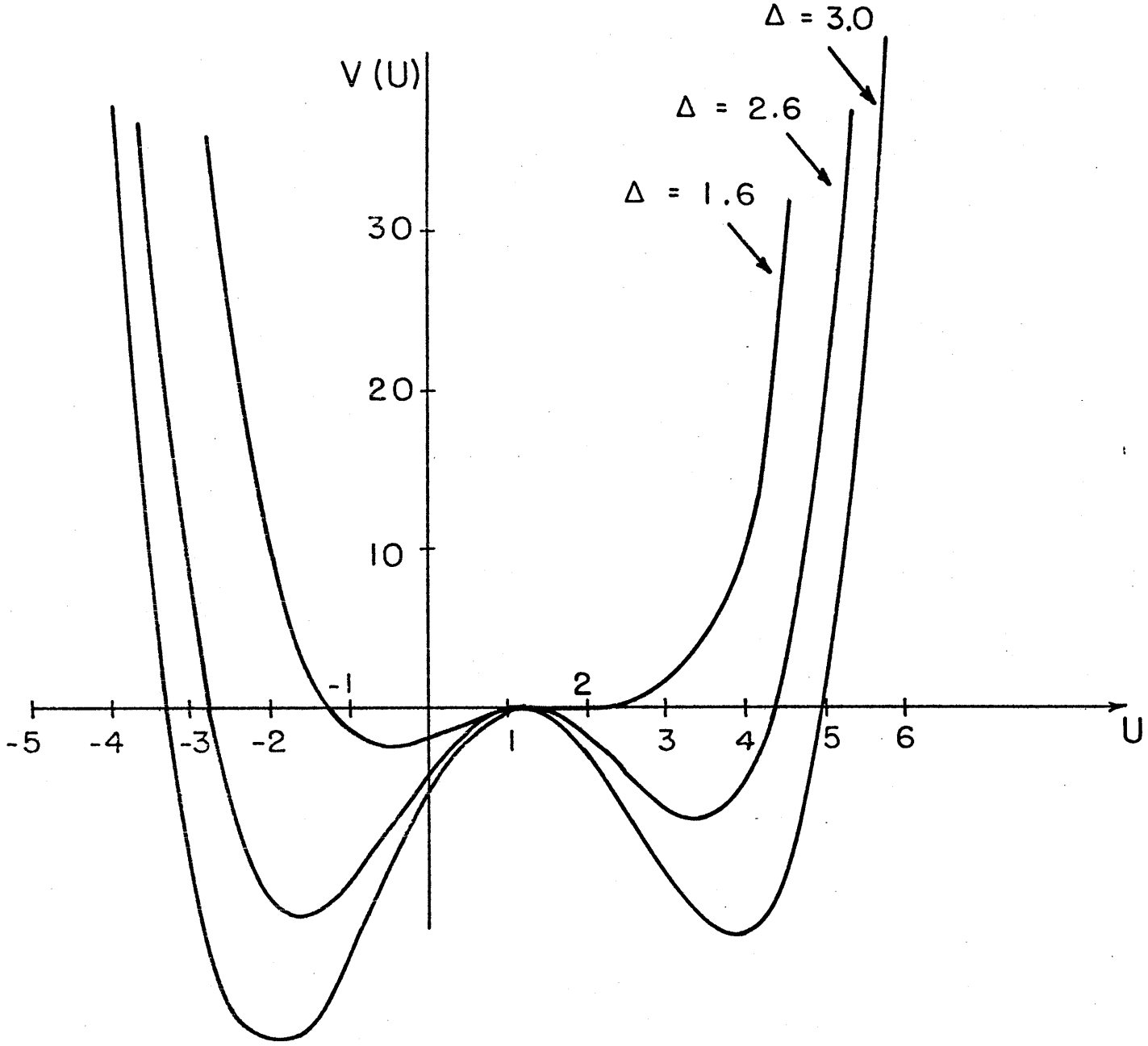
Δ = 3.0
Δ = 2.6
Δ = 1.6
V (U)
30
20
10
-1
2
-5
-4
-3
-2
1
3
4
5
6
U

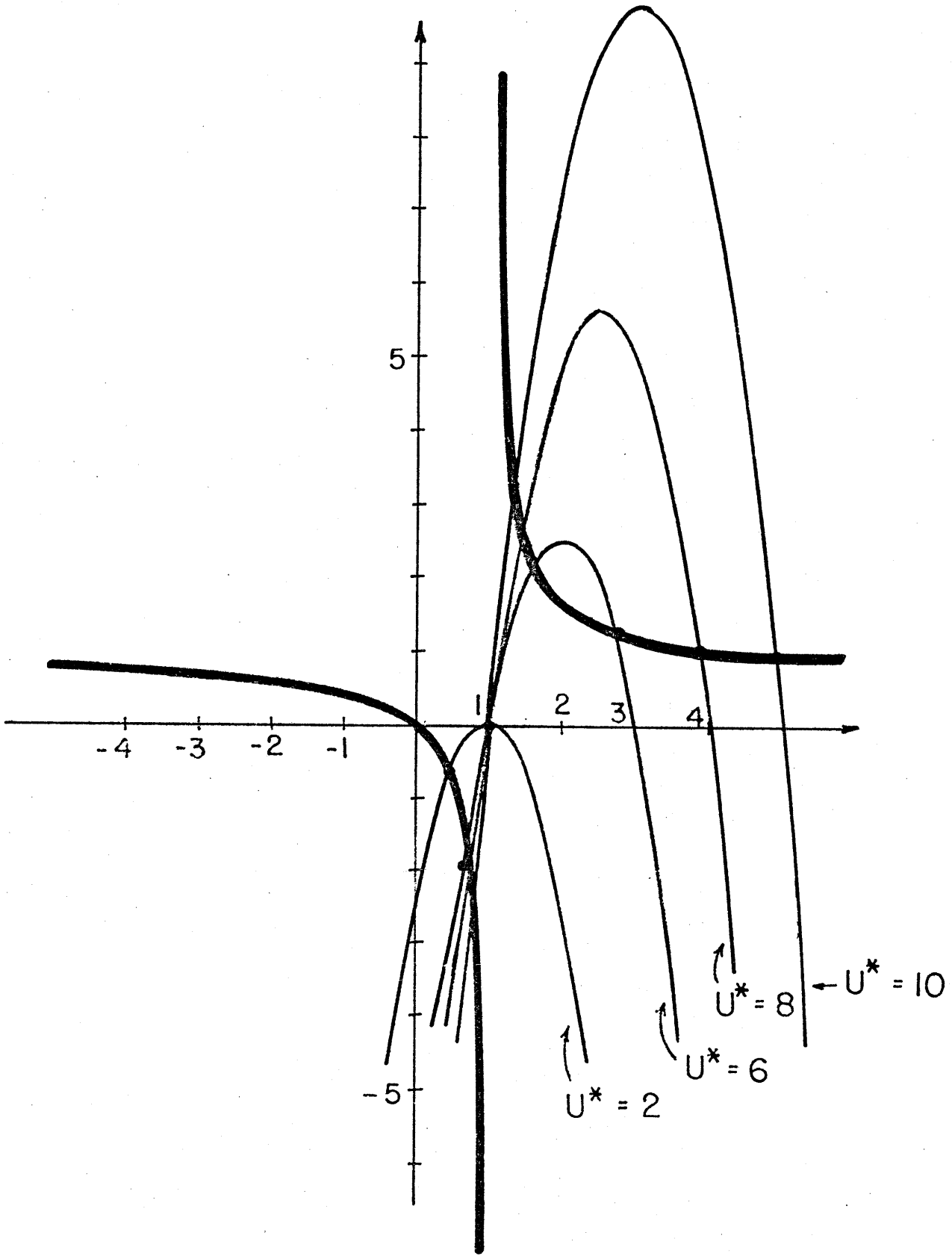
5
-5
-4
-3
-2
-1
1
2
3
4
U* = 2
U* = 6
U* = 8
U* = 10

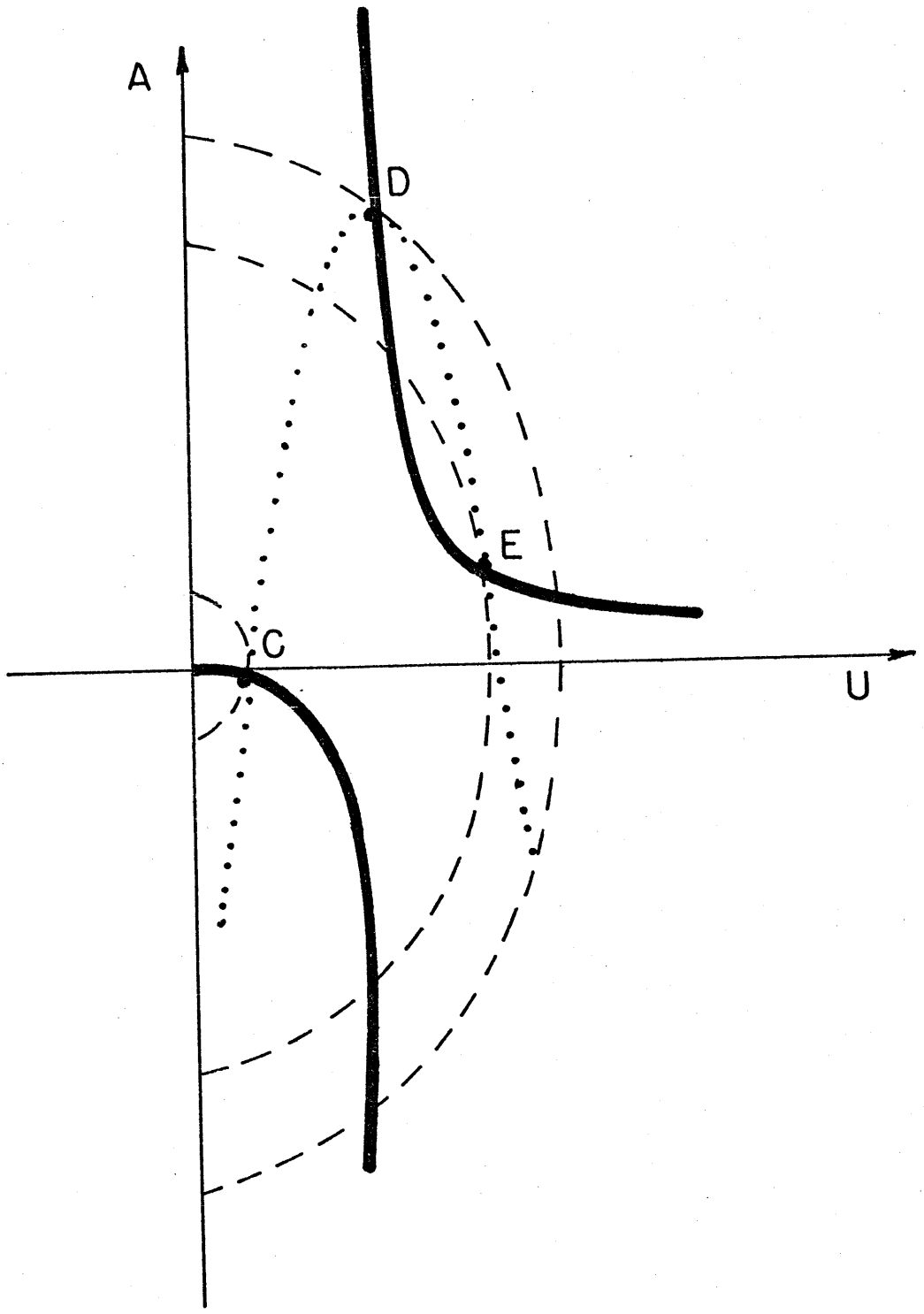
A
D
E
C
U

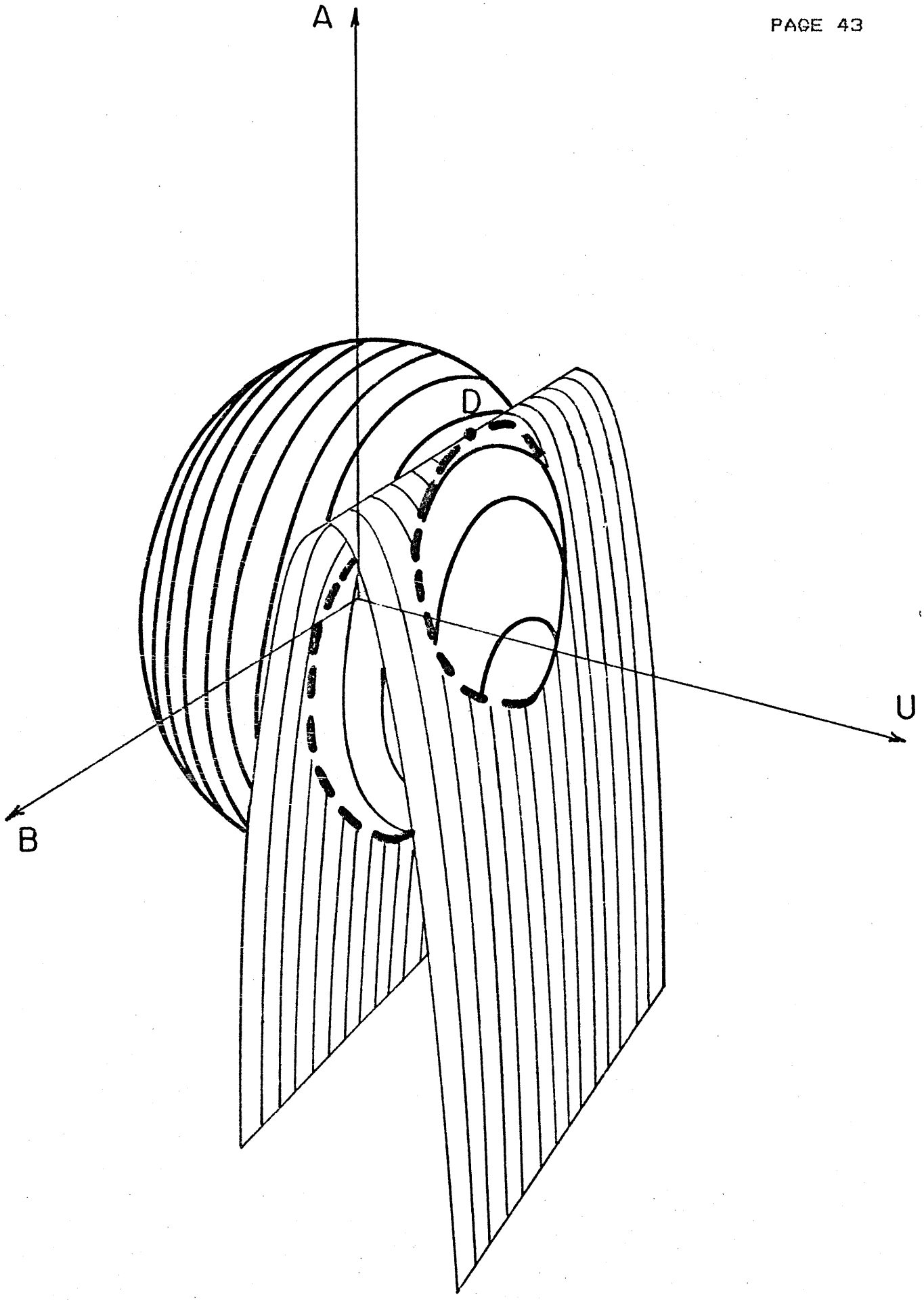
A
D
U
B

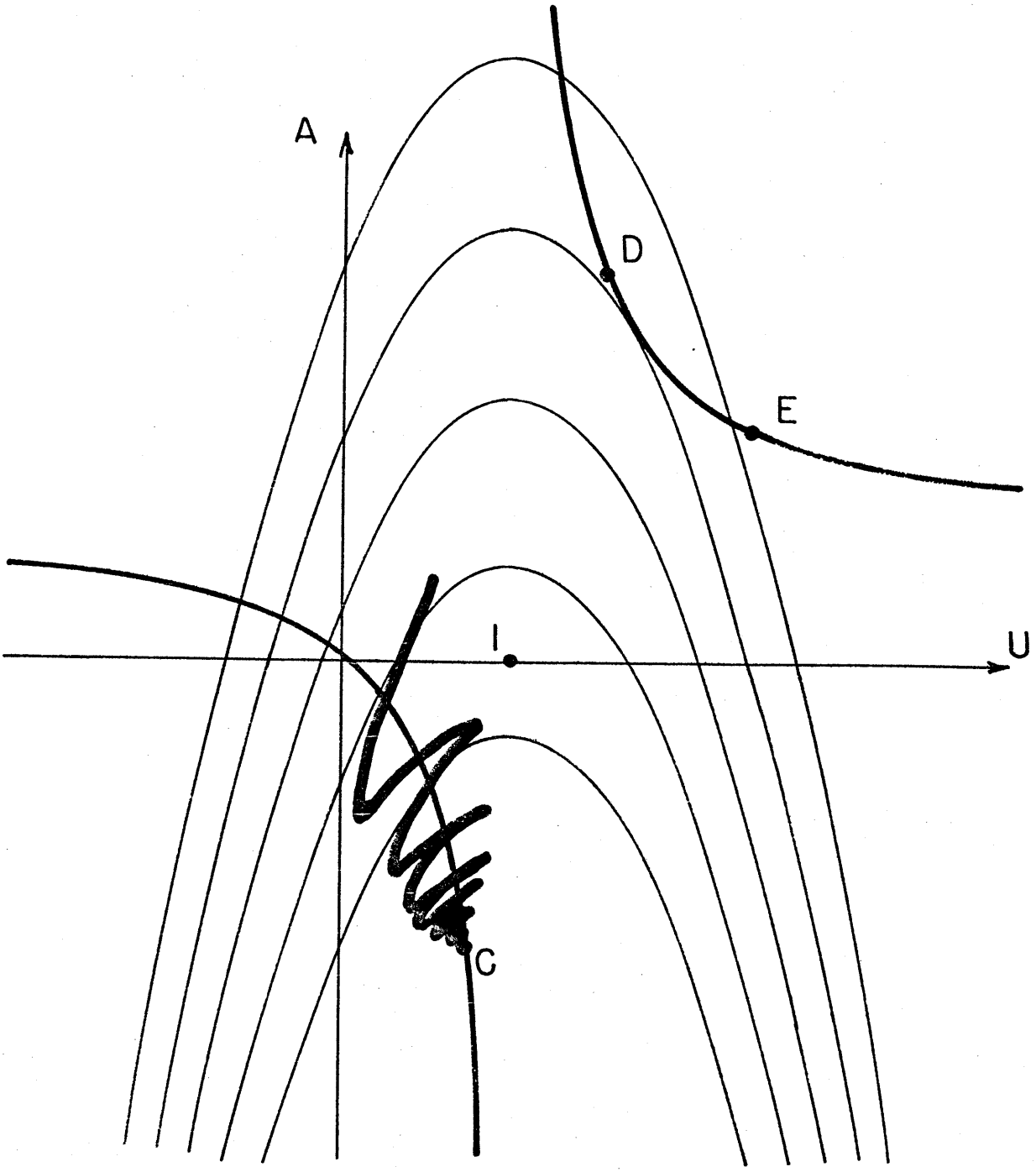
A
D
E
I
U
C

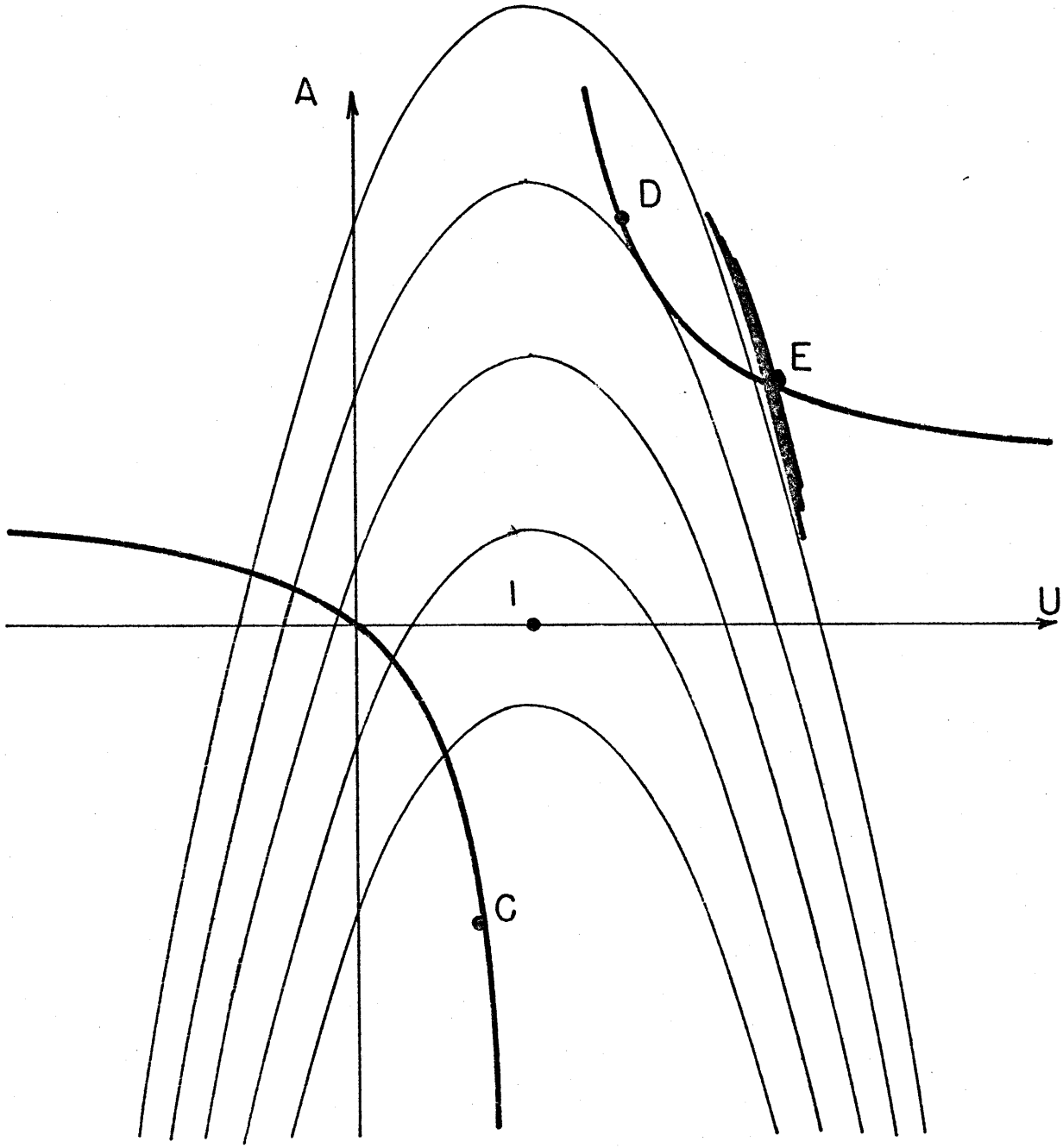
A
D
E
I
U
C

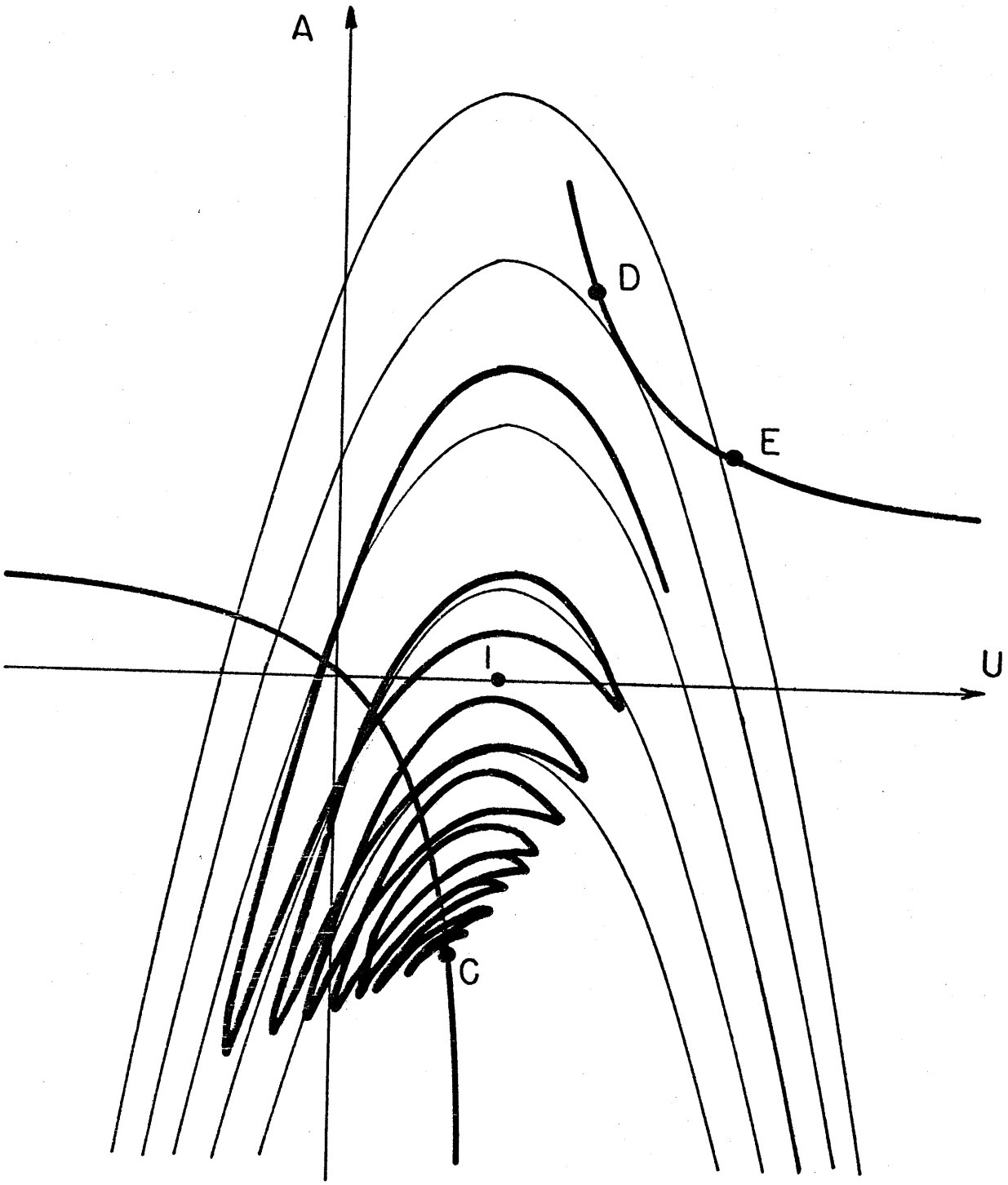
A
D
E
I
U
C

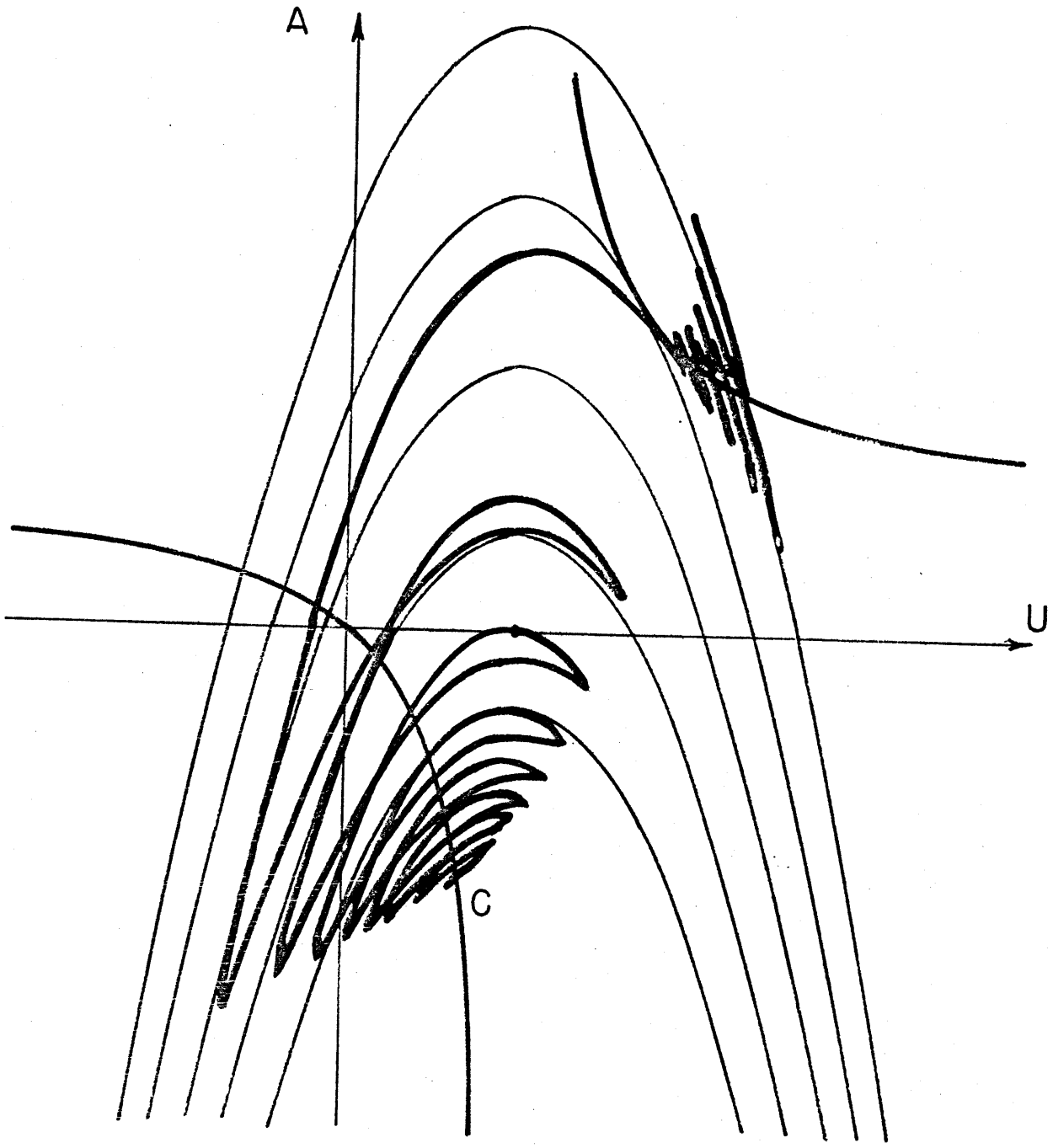
A
U
C

SECTION 2

MULTIPLE EQUILIBRIA IN A BAROCLINIC MODEL

1. Introduction

In the barotropic case the multiplicity of equilibria is due essentially to the resonant structure of the form-drag. Because the form-drag presents a maximum when the speed of the zonal flow goes close to a resonance, $U=\beta/(k^2+l^2)$, the mean zonal flow has the possibility, for a constant external forcing, of reaching different statistical equilibrium values on the two sides of the resonance. From this point of view, we have a strong analogy with the two different equilibrium velocities that an airplane can reach, for a constant propelling force: a subsonic speed or, after having overcome the maximum in the form-drag, a supersonic speed. These general qualitative considerations continue to apply also to the baroclinic case, but here we have some evidence that the equilibria found could be unreachable if the system is too unstable to synoptic scale baroclinic instability (Reinhold, 1981).

We have organized our study in a compact way that allows us to discuss the multiple equilibria problem in a

more general and simple way as function of the external thermal forcing. We have demonstrated that the multiple equilibria suggested by Charney and Straus for realistic parameter values are baroclinically unstable to short waves. We have found that the balance implied by one of the model equations, the barotropic zonal flow equation, is quite different from the real atmospheric balance. We have then shown that a simple correction to this equation, simulating a constant flux of zonal angular momentum from the tropics, leads to more baroclinically stable equilibria. New equilibria are then hypothesized in which the solutions have a large scale stationary part and a synoptic scale time dependent part. this large scale state is near the stability boundary but the synoptic motions also play an important role in the heat and momentum balances.

2. Equations of motion

In the barotropic case it was decided to force the zonal flow directly, arguing that this forcing, in a baroclinic atmosphere, would correspond to the thermal wind driven by the radiation field. To take into account the direct thermal forcing and to study the effects of baroclinicity of the flow, Charney and Straus (1980) decided to look for multiple equilibria in a highly truncated two-layer model. Following their notation, we consider the potential vorticity equations for the two layers

$$\left[\frac{\partial}{\partial t} + J(\psi_1, \cdot)\right] q_1 = -\kappa_d' \nabla^2(\psi_1 - \psi_2) - h_d''\left[(\psi_1 - \psi_2)^* - (\psi_1 - \psi_2)\right] \tag{2.1}$$

$$\left[\frac{\partial}{\partial t} + J(\psi_2, \cdot)\right] q_2 = +\kappa_d' \nabla^2(\psi_1 - \psi_2) + h_d''\left[(\psi_1 - \psi_2)^* - (\psi_1 - \psi_2)\right] - \kappa_d \nabla^2 \psi_2$$

where the subindex 1 indicates the upper layer

the subindex 2 indicates the lower layer

κ_d' represents internal dissipation

κ_d represents bottom Ekman dissipation

λ represents the Rossby deformation radius

The starred quantities represent the external

forcing of the temperature field, here parameterized as a Newtonian relaxation with an inverse time scale of $\lambda^2 h_d''$.

The potential vorticities in the two layers are defined by

$$q_1 = \nabla^2 \psi_1 + \beta y - \frac{1}{\lambda^2}(\psi_1 - \psi_2)$$

$$q_2 = \nabla^2 \psi_2 + \beta y - \frac{1}{\lambda^2}(\psi_2 - \psi_1) + f_0 \frac{h}{H}$$

where h is the height of the topography and H is the mean depth of each layer.

We consider this flow in a channel with meridional walls at y = 0 and y = π L. Let x and y be scaled by L, t by f_0^{-1}, u and v by $L f_0$, ψ by $L^2 f_0$, β by $f_0 L^{-1}$, h by H and define the non dimensional parameters

$$\left(\frac{2L^2}{\lambda^2}, \frac{\kappa_d}{f_0}, \frac{\kappa_d'}{f_0}, \frac{\lambda^2 h_d''}{f_0} \right) = \left(\mu^2, \kappa, \kappa', h'' \right)$$

respectively. To get a spectral model we develop all our variables, now dimensionless, on a complete set of functions, here denoted by $\{F_i\}$, such that $\nabla^2 F_i = -\lambda_i F_i$ and $\overline{F_i F_j} = \delta_{ij}$; we let

$$\beta y = - \Sigma_i \beta_i F_i$$

$$(\psi_1, \psi_2) = \Sigma_i (\psi_{1i}, \psi_{2i}) F_i$$

$$(q_1, q_2) = \Sigma_i (q_{1i}, q_{2i}) F_i$$

$$h = \Sigma_i h_i F_i$$

and we define $\overline{F_i J(F_j, F_k)} = c_{ijk}$ where the bar implies a horizontal average on the channel. Substituting these definitions in (2.1) we get

$$\dot{q}_{1i} + \Sigma_{jk} c_{ijk} \psi_{1j} q_{1k} = \kappa' \lambda_i (\psi_{1i} - \psi_{2i}) - \frac{1}{2} \mu^2 h^* [(\psi_{1i} - \psi_{2i})^* - (\psi_{1i} - \psi_{2i})]$$

(2.2)

$$\dot{q}_{2i} + \Sigma_{jk} c_{ijk} \psi_{2j} q_{2k} = -\kappa' \lambda_i (\psi_{1i} - \psi_{2i}) + \frac{1}{2} \mu^2 h^* [(\psi_{1i} - \psi_{2i})^* - (\psi_{1i} - \psi_{2i})] + \kappa \lambda_i \psi_{2i}$$

where $$q_{1i} = - \lambda_i \psi_{1i} - \beta_i - \frac{1}{2} \mu^2 (\psi_{1i} - \psi_{2i})$$

and $$q_{2i} = - \lambda_i \psi_{2i} - \beta_i + \frac{1}{2} \mu^2 (\psi_{1i} - \psi_{2i}) + h_i$$

An alternative set of variables is usually introduced to discuss the dynamics of the two layers and their interactions: the barotropic and baroclinic components of the stream-function

$$\psi_i = \frac{1}{2}(\psi_{1i} + \psi_{2i})$$

$$\theta_i = \frac{1}{2}(\psi_{1i} - \psi_{2i})$$

and the barotropic and baroclinic component of the potential vorticity

$$(q_\psi)_i = \frac{1}{2}(q_{1i} + q_{2i}) = -\lambda_i \psi_i - \beta_i + \frac{1}{2} h_i$$

$$(q_\theta)_i = \frac{1}{2}(q_{1i} - q_{2i}) = -(\lambda_i + \mu^2)\theta_i - \frac{1}{2} h_i$$

With these new variables the equations of motion (2.1) become

$$\lambda_i \dot{\psi}_i = \Sigma_{jk} c_{ijk}[\psi_j (q_\psi)_k + \theta_j (q_\theta)_k] - \frac{1}{2}\kappa \lambda_i (\psi_i - \theta_i) \tag{2.3}$$

$$(\lambda_i + \mu^2)\dot{\theta}_i = \Sigma_{jk} c_{ijk}[\psi_j (q_\theta)_k + \theta_j (q_\psi)_k] + \frac{1}{2}\kappa \lambda_i (\psi_i - \theta_i) - 2\kappa' \lambda_i \theta_i + \mu^2 h'' (\theta_i^* - \theta_i)$$

In our discussion we shall consider the energy equation obtained from adding the first equation of (2.2) multiplied by ψ_{1i} to the second equation multiplied by ψ_{2i} and summing over i. After changing to the new

variables, the energy equation takes the form

$$\frac{d}{dt}\Sigma_i\left[\lambda_i\psi_i^2+(\lambda_i+\mu^2)\theta_i^2\right]= \\ =-\Sigma_i\left[4\kappa'\lambda_i\theta_i^2+\kappa\lambda_i(\psi_i-\theta_i)^2-2\mu^2h''(\theta_i^*-\theta_i)\theta_i\right] \tag{2.4}$$

We shall also consider the potential enstrophy equations for both layers obtained by summing over i the first equation of (2.2) multiplied by q_{1i} and the second equation multiplied by q_{2i} ; for the upper layer we get

$$\frac{d}{dt}\Sigma_i\frac{1}{2}q_{1i}^2=\Sigma_i q_{1i}\left[2\kappa'\lambda_i\theta_i-\mu^2h''(\theta_i^*-\theta_i)\right] \tag{2.5}$$

and for the lower layer

$$\frac{d}{dt}\Sigma_i\frac{1}{2}q_{2i}^2=-\Sigma_i q_{2i}\left[2\kappa'\lambda_i\theta_i-\mu^2h''(\theta_i^*-\theta_i)-\kappa\lambda_i(\psi_i-\theta_i)\right] \tag{2.6}$$

3. Low-order model

Following the procedure used for the barotropic model to find multiple equilibria we consider only three modes, the same as Charney and Straus (1980; from now on referred as C-S):

a zonal mode

$$F_1 = \sqrt{2}\cos(y) \qquad \lambda_1 = 1$$

and two wavy modes

$$F_2 = 2\sin(y)*\cos(m*x) \qquad \lambda_2 = 1 + m^2$$

$$F_3 = 2\sin(y)*\sin(m*x) \qquad \lambda_3 = 1 + m^2 = \lambda_2$$

This choice, in particular, enables our system to have baroclinic instability and to balance the generation of heat with the divergence of the eddy fluxes of sensible heat. The interaction coefficient between these modes is given by

$$C_{123} = -C = -\frac{8\sqrt{2}}{3\pi}m$$

The β-term has projection only on F_1, $\beta_2 = \beta_3 = 0$, and we choose $\beta_1 = \beta/C$ to match the C-S value;

we consider a single mode topography with projection only on F_2, $h_2 = h$ and $h_1 = h_3 = 0$.

The evolution equations for the zonal flow become

$$\dot{\Psi}_1 = \frac{1}{2} c h (\Psi_3 - \Theta_3) - \frac{1}{2} \kappa (\Psi_1 - \Theta_1) \qquad (3.1)$$

$$(1+\mu^2)\dot{\Theta}_1 = -\dot{\Psi}_1 + c\mu^2(\Psi_2\Theta_3 - \Psi_3\Theta_2) - 2\kappa'\Theta_1 + \mu^2 h''(\Theta_1^* - \Theta_1) \qquad (3.2)$$

In a long time mean we can see from the first equation that, in the lower layer, the form drag must push the zonal flow to balance the dissipation due to the Ekman bottom boundary layer. In this simple model the Reynolds' stresses are identically zero, and from the second equation we can see that the eddy fluxes of sensible heat, the internal dissipation and the Newtonian cooling must balance the external generation of heat.

If complex variables are introduced for the wavy part of the flow:

$$\Psi = \Psi_2 + i\,\Psi_3$$

$$\Theta = \Theta_2 + i\,\Theta_3$$

Eqs. (2.3) can be rewritten as:

$$\lambda_2 \dot{\Psi} = a_{11}\Psi + a_{12}\Theta - b \qquad (3.3)$$

$$(\lambda_2+\mu^2)\dot{\Theta} = a_{21}\Psi + a_{22}\Theta + b \qquad (3.4)$$

where a_{11}, a_{12}, a_{21}, a_{22} and b are functions only of the zonal quantities, Ψ_1 and Θ_1, defined by

$$a_{11} = -\left\{\frac{1}{2}\kappa\lambda_2 + ic[\beta_1 - (\lambda_2-1)\Psi_1]\right\}$$

$$a_{12} = \frac{1}{2}\kappa\lambda_2 + ic(\lambda_2-1)\Theta_1$$

$$a_{21} = \frac{1}{2}\kappa\lambda_2 + ic(\lambda_2-1-\mu^2)\Theta_1$$

$$a_{22} = -\left\{\frac{1}{2}\kappa + 2\kappa' + \mu^2 h'' + ic[\beta_1 - (\lambda_2-1+\mu^2)\Psi_1]\right\}$$

$$b = \frac{1}{2}ic\,h\,(\Psi_1 - \Theta_1)$$

4. Multiple equilibria

Without the topography this system has a simple behavior. For a small forcing it has a stable stationary solution, with no waves and with the heat balance satisfied by the mean meridional circulation; if the forcing is increased this solution becomes unstable to baroclinic instability and the system reaches a different stable equilibration with the meridional temperature gradient set to the two-layer critical value for baroclinic instability and with a translating baroclinic wave large enough to transfer all the heat necessary to balance the external forcing. This second state corresponds to a stable cycle in the phase space.

The presence of topography enriches the system with several new behaviors and, as C-S discussed, it can show stationary, periodic or aperiodic solutions, depending on the range of parameters chosen and on the initial conditions.

In this paper we shall mainly consider the stationary solutions and their stability.

To compute stationary solutions Eqs. (3.1)-(3.2)-(3.3)-(3.4) are solved without the time dependence. A graphical solution in the plane (ψ_1 , θ_1) is presented in Fig. 1. This is obtained by computing at each point (ψ_1 , θ_1) the wavy part, from Eqs. (3.3)-(3.4)

which are linear once the zonal flow is specified, then computing the external forcing θ_1^* from Eq. (3.2) (the light lines represent curves of constant θ_1^*), and finally looking for the points where the form-drag and the Ekman dissipation are in balance (heavy lines), Eq. (3.1). The straight heavy line at forty five degrees represents the Hadley solutions with no wave present and with zero wind speed in the lower layer; the closed heavy line represents non trivial balances between form drag and dissipation.

The intersections between the heavy lines and a selected light line define the stationary solutions for a selected strengh of forcing .

In the case here studied the external parameters have been set to the following values:

πL = 5000 Km channel width

H = 5 Km mean depth of each layer

λ = 1000 Km Rossby deformation radius

$\mu^2 = 2L^2/\lambda^2 = 5.$

The internal and Ekman dissipation time scales as well as the Newtonian heating time scale have been set to ten days corresponding to:

$\kappa = \kappa' = h'' = .0114$

For the topographically forced wave we have chosen zonal wave number three, $n = 3$ and $m = (n/2.83)$, and the amplitude of the sinusoidal topography has been set to 1 Km.

With these choices we get the same equations with the same parameter values as C-S.

Before discussing the stationary solutions of the full system it is useful to consider the stationary waves that are forced by the topography for a fixed (ψ_1 , θ_1). In Figs. 2 and 3 the amplitude and the phase, relative to the topography, of the barotropic and baroclinic forced waves are drawn. Because the topography interacts only with the lower-layer flow we also present the amplitude and the phase of the forced wave on this layer (Fig. 4). The straight line $\psi_1 = \theta_1$ divides the plane in two regions; in the upper part the zonal flow has easterlies while in the lower part it has westerlies in the lower-layer. The region of positive form drag, where the topography pushes the zonal flow eastward (i.e., the phase is between $-\pi$ and 0), have been shaded (Fig. 4b).

As we can see the amplitude of the forced solutions is dominated by the intensity of the zonal flow in the lower layer, $(\psi_1 - \theta_1)$, and by the presence of a resonant curve. In the inviscid case this resonant curve (heavy line of Fig. 5) is the two-layer baroclinic extension of the resonant barotropic point, $\theta_1 = 0$ and $\psi_1 = \dfrac{\beta}{\lambda_2 - 1}$; and in particular

it can be shown that, for westerly flows in the interior of this semicircle (shaded region), the barotropic and the baroclinic forced waves are in phase with the topography, with cyclonic curvature on the peaks and anticyclonic curvature in the valleys, as in the barotropic subresonant case.

It is interesting to point out that the system (3.3)-(3.4) has a true resonance, infinite response, even in the presence of dissipation. In fact there is a point $\overline{P}$ that lies on the closed heavy line of Fig. 1, where the dissipation is balanced by the generation and it is possible to have a stationary wave also without the topography; of course, this stationary solution cannot be reached for a finite value of the external forcing θ_1^*. We find a resonance when the determinant of coefficients of Ψ and $\textcircled{H}$, Eqs. (3.3)-(3.4), vanishes.

$$a_{11} a_{22} - a_{21} a_{12} = 0$$

The real part vanishes on the heavy line of Fig. 5 while the immaginary part vanishes on the dashed line; the intersection between this two curves defines the position of the infinite resonance. Thus unlike the barotropic case where the amplitude of the wave is limited by dissipation as

the forcing is increased, the stationary wave amplitudes here grow as $\sqrt{\theta_1^*}$ when the forcing is increased.

Due to the presence of this true resonance we can anticipate that in its neighborhood the forced stationary wave are large enough to tranfer meridionally all the heat necessary to balance the external heat forcing and therefore we can expect multiple equilibria. As we can see, after having solved the problem, (Fig. 1) for small values of the forcing ($\theta_1^* < .140$) we have only one intersection corresponding to a stable direct Hadley circulation, without any forced wave. For values of the forcing between .140 and .175 two new equilibria are present; one has easterly zonal wind ($\psi_1 > \theta_1$) in the lower layer and the forced waves exert a negative form drag while the other has westerly zonal wind ($\theta_1 > \psi_1$) in the lower layer and the forced waves exert a positive form drag. For values of the forcing between .175 and .200 two other equilibria appear; for $\theta_1^* < .195$ both have westerlies and for $\theta_1^* > .195$ one has easterlies at the ground. When the forcing is increased further, the two solutions with easterlies disappear leaving three equilibria. One is the Hadley solution that has only a mean meridional circulation and, as we can see, is not very efficient in transfering heat meridionally and therefore gives meridional temperature gradients θ_1 close to the forced ones θ_1^*. The other two equilibria are locked to

the true resonance and, in analogy with the barotropic case, one can be called subresonant and the other superresonant, depending on whether it is inside or outside the resonant curve of Fig. 5.

Before continuing our study of these equilibria, let us try to state why these equilibria are important and from which characteristics they get their importance.

The presence of equilibria points or, more generally, the existence of regions in the phase space where some components are slowly varying, increases the predictability of these components. In our case these are the mean zonal flow and those modes directly forced by the topography. Following Speranza (private comunication) these regions can be seen as examples of islands of predictability in a stochastic, unpredictable space. In our case, because we are considering stationary solutions, the high predictability is a consequence of the high persistence.

There are four classes of persistence islands that we can find:

a) * Stable stationary solution * In the most simple and fortunate case we could find a full stationary stable solution, for which the system remains confined inside its attractor basin, once it gets there.

b) * Unstable stationary solution * In a still

simple case we could find a full non-linear stationary solution with some linearly unstable eigenvectors. In this case, once the system is close enough to the equilibrium point, it continues to go closer in some directions, on the stable manifold, while along others, on the unstable manifold, it departs. Once the system enters the region of validity of the linear stability theory around such equilibrium, its persistence , i.e., the amount of time that the system spends close to this point becomes directly related to the amplitudes of the most unstable eigenvectors and the values of their growth rates. The unstable stationary points of the Lorenz system in the aperiodic regime are examples of this case.

c) * Stable quasi-stationary solution * This corresponds to a stable solution with only some components stationary or nearly stationary, where this quasi-stationarity is due to the non-linear interaction with the full non-stationary components. A stable cycle with some constant components is a simple example of this case.

d) * Unstable quasi-stationary solution* In the more general case we can find an unstable solution with only some components nearly stationary. Here, to understand the time behavior of the system in the neighborhood of this point, we have to consider the instability of this state

taking into account the role of the non-stationary components.

We do not have any evidence that full stationary solutions do exist, but we have some experimental evidence - blocking situations - and some theoretical suggestions - multiple equilibria theory - of the existence of solutions with a non trivial quasi-stationary part. The solutions that have been found until now have been obtained with spectral highly truncated models and, therefore, must be seen only as possible approximations to real persistent solutions. Here we still have an open question on the validity of these stationary truncated solutions, but we realize that these solutions can be very relevant even if they are only approximations of unstable quasi-stationary solutions.

Once the system is supposed to be in the presence of one of these islands we still have to determine its impact on the time behavior of our system. An island gets its importance from the amount of time spent by the system in its neighborhood and this is a function of the extent of the attractor basin in its stable manifold and on the growth rates present in the unstable manifold.

Here we conclude our general considerations and believing that our truncated stationary solutions are approximations of real quasi-stationary solutions we

continue our study. To begin our understanding of the unstable manifold around the C-S stationary solutions we shall study the linear "internal" instabilities in the subspace including only the forced waves and the zonal flow and then we shall consider some "external" instabilities in the subspace containing the most unstable baroclinic wave.

Let us first consider the "internal" instabilities of these stationary solutions, i.e., perturbations in the zonal flow and in the wave field with the same zonal and meridional wave number of the topography, described by the system of Eqs. (3.1)-(3.2)-(3.3)-(3.4) linearized around the chosen stationary solution. As we shall see, as a consequence of the introduction of another external forcing, all the points (Ψ_1, θ_1) can correspond to stationary states; therefore we compute the growth rates of the unstable modes on the whole plane. We have a sixth-order eigenvalue problem with real coefficients. The number of unstable roots is plotted in Fig. 6a and the number of unstable non propagating (real) roots is plotted in Fig. 6b. Without the topography we do not find any finite area region of growing stationary perturbations; there is only a line (dashed line in Fig. 6b) that divides the eastward propagating from the westward propagating ones. As we see, while this line now has been broadened to a region of finite area new regions of orographic instabilities (here defined

as instabilities that grow in place) have appeared. In Fig. 7 we have plotted isolines of the largest growth rate in presence of topography. In Fig. 8 we have plotted isolines of the largest growth rate obtained, solving the same instability problem without topography; in this case the basic state that we perturb has no wave and we have pure baroclinic instability. As we can see the barotropic part of the flow influences the growth rate as well as the phase speed of the perturbation: this is because the mode describing the zonal flow always vanishes at the two walls and a change in the barotropic part is not equivalent to a Galileian transformation. Comparing Fig. 7 with Fig. 8 we see the presence of a strong orographic instability that dominates the picture for low values of the baroclinic zonal flow near the true resonance. The indentation on the isolines in the upper part of the figure shows the stronger influence of the topography on those unstable modes that, also without topography, were growing almost in place. In presence of orography (Fig. 7) we have essentially two kinds of instabilities: for high values of θ_1 we have almost pure baroclinic instability and the source of the perturbation energy is the available potential energy of the zonal flow; for low value of θ_1 and close to the true resonance we have almost a pure orographic instability and the forced stationary wave is the main source of energy for

the instability as in the super-resonant barotropic case. The heavy line of Fig. 7 indicates the stationary solutions of the C-S model for different values of the forcing and we see that some of these solutions are stable, or weakly unstable, to "internal" perturbations (same wavenumber as topography), suggesting that, if these are the dominant instabilities, some of these equilibria can play an important role in the time behavior of the system.

At this first level of truncation we could still find a stable stationary solutions. Another subspace that has been studied by C-S is the one including modes with the same zonal wave number of the topography, but with a higher meridional wave number; they found that all their stationary solutions were unstable to these perturbations. The effects of this higher y-mode instability have been studied by Arakawa and his collaborators (private comunication) who ran a two-layer highly truncated spectral model including one zonal wave number and three meridional ones; they found that, instead of multiple stationary solutions, multiple statistical steady states can be reached resembling the C-S multiple equilibria. In this way they have shown that these instabilities are not able to take and to keep the system completely away from the equilibria but they weakly modify the equilibration. In particular, these unstable modes participate in the meridional heat transfer

lowering the equilibrium value meridional temperature gradient. At this second level of truncation they show that there may be stable quasi-stationary solutions.

Serious concerns about the importance of the C-S multiple equilibria arise when we consider the subspace containing the most unstable baroclinic wave. With the parameters chosen in this model the most unstable baroclinic wave has the largest meridional wave lenght and zonal wave number five. To consider its influence we neglect the direct topographic forcing on the most unstable baroclinic wave with zonal number five and we study a new instability problem, adding to Eq.s (3.1)-(3.2)-(3.3)-(3.4) the analogous equations for zonal wave number five. This problem can be factored in two sub-problems: the first describing the zonal flow and the topographic forced waves that we have just studied and the second describing the instability of wave number five in a constant zonal flow. In Fig.9 we have plotted isolines of the largest growth rate obtained in this second problem (no topography and zonal wave number five). To understand the stability of the C-S stationary solutions for the most unstable baroclinic wave we have superimposed the curve that delineates the C-S stationary states for different values of the forcing in Fig.9 (heavy lines). As we can see only the Hadley solution for small value of the forcing is stable.

Stone (1978) has shown that at middle latitudes the real atmosphere is very close to the neutral value for baroclinic instability in the two-layer model, and the same result has been confirmed with a numerical time integration of a two-layer model. The fact that the C-S stationary solutions require a meridional temperature gradient almost twice as big raises some suspicions about their importance, and indeed it has been shown (Reinhold, 1981) that the system does not stay close to any of these multiple equilibria. To prove the preceding point Reinhold used a two-layer highly truncated model including the zonal flow and two zonal wave numbers, one directly forced by the topography and another more baroclinicly unstable, with two meridional wave numbers, to allow some non-linear interactions.

5. Search for more stable equilibria

From Fig. 9 we have seen how all the C-S wavy equilibria are strongly baroclinically unstable. To understand if this negative result is a consequence of some neglected important physical phenomena, we studied the assumptions of the C-S model. We started by considering the parameters involved and, as pointed out by Reinhold, we verified that this model is sensitive to reasonable changes in the parameters, but is also very consistent in producing multiple equilibria which are strongly baroclinically unstable.

To understand the reason for their instability we must understand why the non-trivial balances between form drag and dissipation are obtained only for high values of θ_1. Because this is a complex balance we did not find a simple explanation and we decided to compare this balance in our model with the one in the real atmosphere.

The model equation (3.1) states that, in equilibrium or in a long time average, the mountain acts to balance the dissipation of zonal momentum due to the surface Ekman boundary layer. This statement does not agree with the observational studies on the relative role of mountain torque and surface friction. Newton (1971) and Oort and Bowman (1974) found that, on the average, the mountain torque and the surface friction work together against the

convergence of angular momentum flux, the Reynolds' stresses neglected in our model.

It is interesting to point out that this problem is not present in the barotropic studies where the zonal flow is directly forced, and also that if we compute the convergence of momentum necessary to give the zonal forcing used by Charney and DeVore (1979), we get a somewhat higher but still realistic value of the atmospheric convergence of momentum due to Reynolds' stresses. In Table 1 we have computed the barotropic and baroclinic convergence of eddy flux of angular momentum in the latitudinal band from 30° to 60° N for the extreme seasons using the data of Oort and Rasmusson (1971); for this calculation we divided the atmosphere in two layers, one from the ground to 500 mb and the other from 500 mb to 50 mb. As we can see the tropics are a source of both barotropic and baroclinic angular momentum for the mid-latitudes, and these momentum exchanges (that are neglected in channel models when the meridional boundary condition, $v = 0$, is applied) can play an important role on our stationary solutions.

To take this momentum source for the zonal flow into account we decided to include a constant forcing, (F_ψ^* , F_θ^*), in the barotropic and baroclinic zonal momentum equation:

$$\dot{\psi}_1 = \frac{1}{2} ch (\psi_3 - \theta_3) - \frac{1}{2} \kappa (\psi_1 - \theta_1) + F_\psi^* \qquad (5.1)$$

$$(1+\mu^2)\dot{\theta}_1 = -\dot{\psi}_1 + c\mu^2 (\psi_2 \theta_3 - \psi_3 \theta_2) - 2\kappa' \theta_1 + \mu^2 h'' (\theta_1^* - \theta_1) + F_\theta^* \qquad (5.2)$$

The balance for the barotropic part becames now more realistic and we can have stationary states where mountain torque and friction work together to balance the momentum flux convergence. To discuss the effects of this forcing we looked for the equilibria solving for F_ψ^* in the (ψ_1, θ_1) plane. The balance for the baroclinic zonal flow is not so drastically influenced; in fact the flux of baroclinic zonal momentum simply adds its contribution to the external radiation forcing in trying to set a larger vertical shear and we can simply continue our discussion by introducing a new effective forcing θ_e^* given by $\theta_1^* + \frac{F_\theta^*}{\mu^2 h''}$. However the discussion of the baroclinic flux of momentum will no longer be so simple once this quantity is parameterized as function of the wave field. Presumably as F_ψ^* becomes less than F_θ^*, the form drag will have to become positive; however the data suggests that this is not the parameter range of atmospheric interest, since the momentum forcing is positive in the lower layer. In Fig. 10 the intersections between a selected heavy line (F_ψ^* = const) and a selected light line (θ_e^* = const) define the stationary solutions for

the particular values of the forcings θ_e^* and F_ψ^*. As we can see the equilibria move in the right direction, becoming more baroclinicly stable and, for realistic values of the zonal momentum forcing, we start to have, in the lower left side of Fig. 10, equilibria with considerable energy in stationary long waves which are baroclinicly stable for shorter, synoptic-scale waves.

Along with the other factors that have been taken into account, we want to mention that changes in the ground friction parameterization (extrapolation to the ground instead of lower layer value being used to compute the Ekman dissipation, i.e., the Ekman term $K_d \nabla^2 \psi_2$ in Eq. (2.1) has been replaced by $\frac{1}{2} K_d \nabla^2 (3\psi_2 - \psi_1)$) improve, but not to the point of stability, the stability of the wavy equilibria (Fig. 11).

Another interesting physical term until now neglected, being difficult to parameterize, but which can play a role in the stabilization of our equilibria, is the latitudinally varying heat forcing due to radiation and moist convection. To get an idea of the sensitivity of our equilibria to non-symmetric heat forcing we considered a simple Newtonian perturbation with the same zonal wave number as the topography, i.e., we introduced a wavy forcing term θ_e^* in Eq. (2.3). In Fig. 12a, b, c, d we present the equilibria obtained for a strong zonally varying heat forcing. The amplitude of the forced wave is 40° K and the

Newtonian time scale is ten days, with different phase relations between the topography and the heat forcing. From Fig. 12b we have the suggestion that when the heating is in phase with the topography multiple equilibria which are baroclinicly stable can be obtained.

6. Conclusion

We have seen how, taking into account in a simple way the fluxes of angular momentum from the tropical regions, our highly truncated two-layer system can have stationary forced large scale waves stable with respect to the baroclinic instability of shorter synoptic scale waves. This state requires a barotropic zonal flow about twice the baroclinic zonal flow in reasonable agreement with what we measure in the real atmosphere.

To discuss the properties of this equilibrium state, varying θ_e^* and F_ψ^*, we consider a low order model with only one meridional wave number and with two zonal wave numbers: a planetary topographically forced wave, zonal wave number three, and the most baroclinically unstable wave, zonal wave number five in our model.

For small value of the tropical forcing F_ψ^* the equilibria obtained with a stationary wave number three and with no wave number five are strongly baroclinically unstable, $\theta_e^* > \theta_1^c$ (where θ_1^c is the neutral value for baroclinic instability, dashed line of Fig. 10), and therefore the shorter wave develops and keeps the value of θ_1 close to θ_1^c preventing the forced long wave from reaching its equilibria.

When we increase F_ψ^* and the isoline F_ψ^* = constant becomes tangent to $\theta_1 = \theta_1^c$ (dashed line of Fig. 10), we have

two situations depending upon the strength of the external radiation forcing. For values of θ_e^* less than θ_1^{*c} (the value of θ_1 on the intersection between $\theta_1 = \theta_1^c$ and the isoline of F_ψ^*) we can have a stationary solution in which the long stationary wave is the only wave present and it transports meridionally all the heat necessary to balance the external radiation forcing and keeps the meridional temperature gradient below the critical value for baroclinic instability. For values of θ_e^* greater than θ_1^{*c} the long forced wave reaches the equilibrium state at the intersection between the isoline F_ψ^* = constant and θ_1^{*c} while the shorter baroclinic wave reaches an amplitude large enough to transfer the heat required to balance the difference between θ_e^* and θ_1^{*c}.

We have explored the possibility of the atmospheric system reaching states in which long stationary waves are present and we have found that a determinant factor for the realization of such a state is the presence of a barotropic zonal momentum flux coming from the tropics into the mid-latitudes. This angular momentum flux is especially strong in winter when examples of atmospheric blocking are more frequent.

REFERENCES

Charney, J.G., J.G. DeVore, 1979: Multiple flow equilibria in the atmosphere and blocking. J. Atmos. Sci., 36, 1205-1216.

Charney, J.G. and D.M. Straus, 1980: Form-drag instability, multiple equilibria and propagating planetary waves in baroclinic, orographically forced, planetary wave systems. J. Atmos. Sci., 37, 1157-1176.

Newton, C.W., 1971: Mountain torques in the global angular momentum balance. J. Atmos. Sci. 28, 623-628.

Oort, A.H., and Bowman II H. D., 1974: A study of the mountain torque and its interannual variations in the northern hemisphere. J. Atmos. Sci. 31, 1974-1982.

Oort, A.H., and E.M. Rasmusson, 1971: Atmospheric circulation statistics. NOAA Prof. Paper 5, Govt. Printing Office, 323 pp.

Reinhold, B.B., 1981: Dynamics of weather regimes: quasi stationary waves and blocking. Ph.D. Thesis, M.I.T., Cambridge, Mass. 02139.

Stone, P.H., 1978: Baroclinic adjustment. J. Atmos. Sci. 35, 561-571.

FIGURE CAPTIONS

Figure 1 : Graphical solution of the equilibria in the plane (ψ_1 , θ_1), the light lines represent lines of constant θ_1^*, the heavy line indicates balances between the form drag and the Ekman dissipation.

Figure 2a: Amplitude of the barotropic forced wave in non-dimensional units.

Figure 2b: Phase, relative to topography, of the barotropic forced wave.

Figure 3a: Amplitude of the baroclinic forced wave in non-dimensional units.

Figure 3b: Phase, relative to topography, of the baroclinic forced wave.

Figure 4a: Amplitude of the forced wave in the lower layer in non-dimensional units.

Figure 4b: Phase, relative to topography, of the forced wave in the lower layer.

Figure 5 : Resonant curve for our two layer channel model without dissipation (heavy line). In presence of dissipation there is still a line on which the dissipative effects balance and in P we therefore have a true infinite response.

Figure 6a: Number of "Internal instabilities". In the white areas we have no unstable roots, while in the other regions we find 1,2 or 3 unstable roots as written.

Figure 6b: Number of "Internal instabilities" with zero phase velocity. In the white areas we have no stationary unstable roots, while in the other regions we find 1,2 or 3 unstable stationary roots as written . The dashed line represents the only unstable stationary root in absence of topography.

Figure 7 : Largest growth rate for the "internal instability". The heavy line, representing balances between form drag and Ekman dissipation, indicates possible equilibria.

Figure 8 : Largest growth rate for the "internal instability" without topography; i.e. growth rate for the baroclinic instability of wave number three.

Figure 9 : Largest growth rate for the most unstable baroclinic mode present in our channel model: zonal wave number five.

Figure 10: Graphical solution of the equilibria in the plane (ψ_1 , θ_1) in presence of a zonal momentum forcing F_ψ^*, the light lines represent lines of constant θ_e^*, the heavy line represent lines of constant ψ_1^*, where $\psi_1^* = F_\psi^*/K$

Figure 11: As in Fig. 10 but with ground extrapolation to compute the Ekman dissipation.

Figure 12a: Graphical solution of the equilibria in the plane (ψ_1 , θ_1) in presence of a zonal momentum forcing F_ψ^*, and a latitudinal Newtonian heat forcing (with amplitude of 40° and a Newtonian time scale of ten days). The heating is in phase with respect to the topography. The

light lines represent lines of constant θ_e^*, the heavy lines represent lines of constant ψ_1^*, where $\psi_1^* = F_\psi^*/K$

Figure 12b: As in Fig. 12a but here the heating is out of phase with respect to the topography.

Figure 12c: As in Fig. 12a but here the heating is leading the topography by 90°.

Figure 12d: As in Fig. 12a but here the heating is behind the topography by 90°.

TABLE CAPTION

Table 1 : Barotropic and baroclinic eddy flux of angular momentum and its convergence between 30° and 60° north. in m/sec (or in our non-dimensional units).

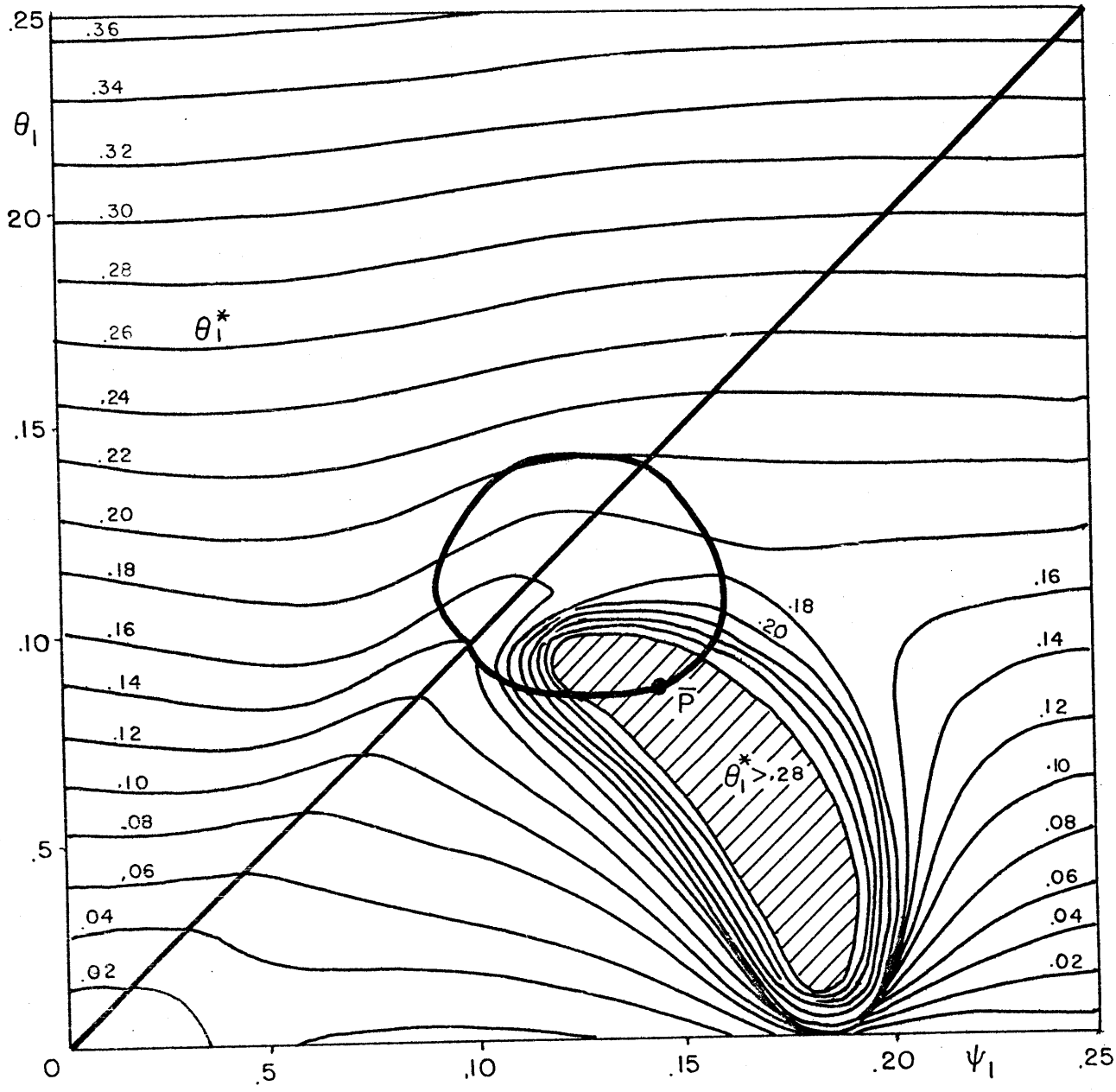
.25
.36
.34
θ_1
.32
20
.30
.28
.26
θ_1^*
.24
.15
.22
.20
.18
.16
.10
.14
.12
.10
.08
.5
.06
.04
.02
0
.5
.10
.15
.20
ψ_1
.25
.18
.20
.16
.14
.12
.10
.08
.06
.04
.02
$\bar{P}$
$\theta_1^* > .28$

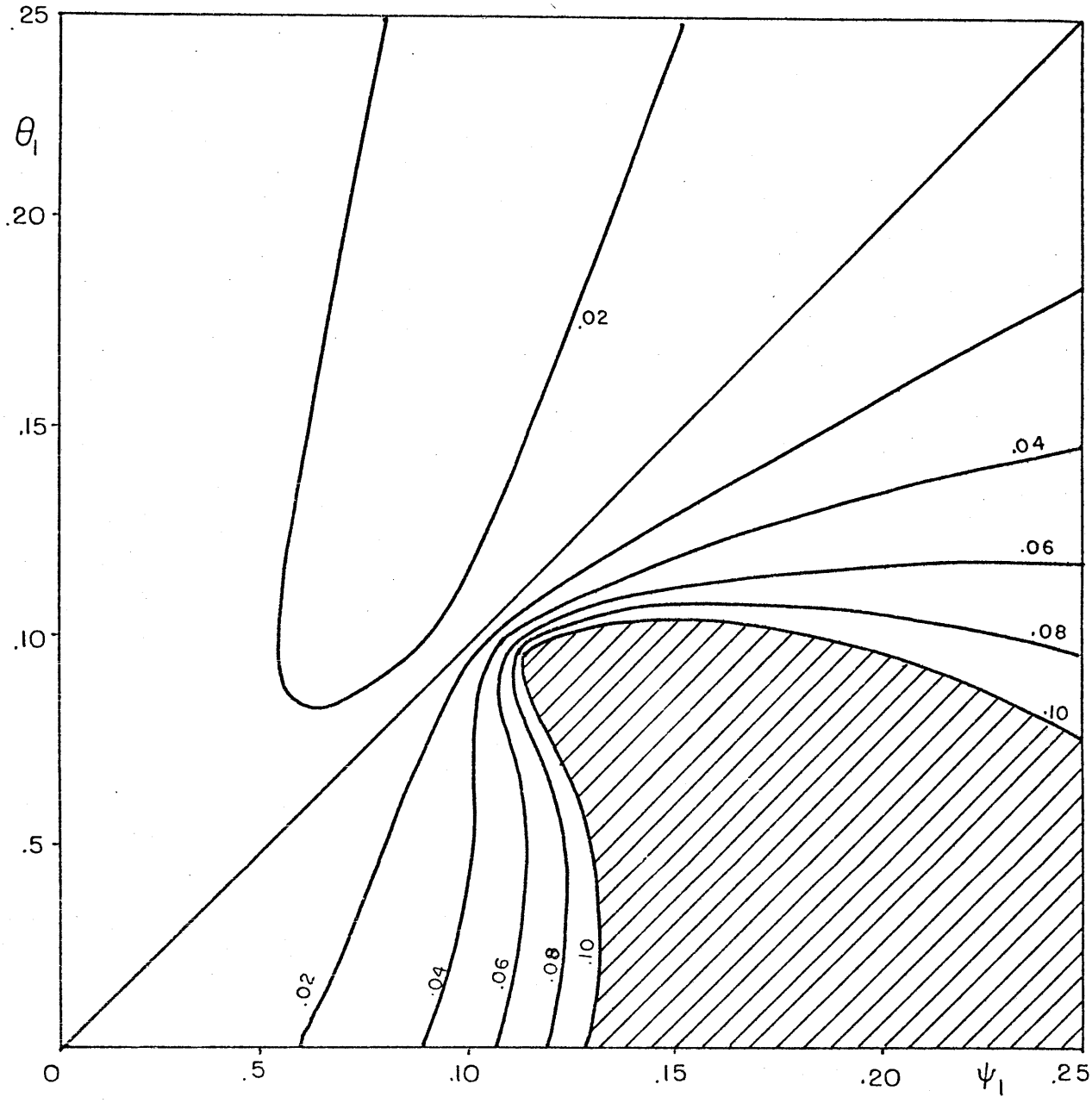
.25
θ_1
.20
.15
.10
.5
0
.5
.10
.15
.20
ψ_1
.25
.02
.04
.06
.08
.10
.02
.04
.06
.08
.10

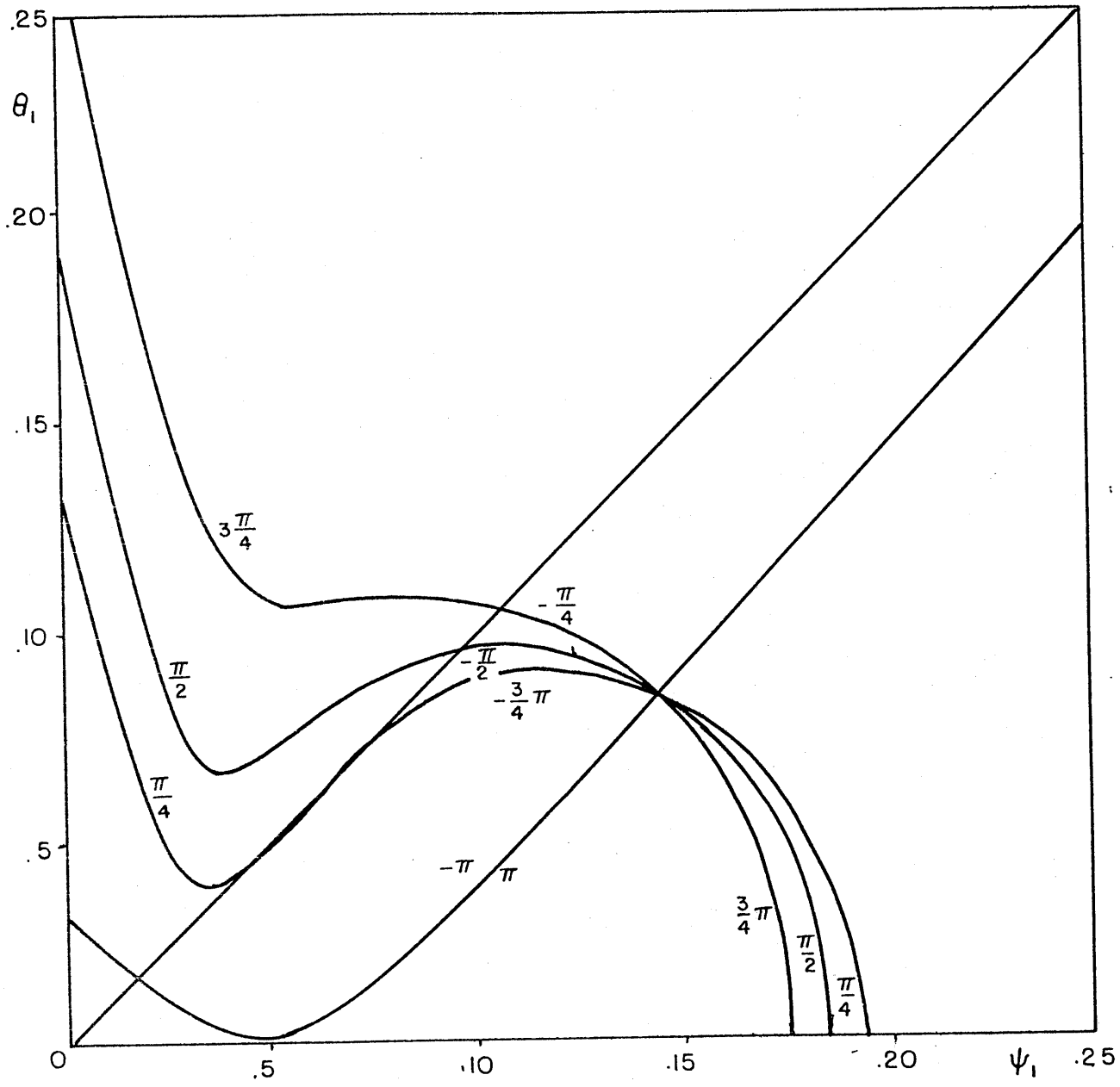
.25
θ_1
.20
.15
.10
.5
0
.5
.10
.15
.20
ψ_1
.25
$3\frac{\pi}{4}$
$\frac{\pi}{2}$
$\frac{\pi}{4}$
$-\frac{\pi}{4}$
$-\frac{\pi}{2}$
$-\frac{3}{4}\pi$
$-\pi$
π
$\frac{3}{4}\pi$
$\frac{\pi}{2}$
$\frac{\pi}{4}$

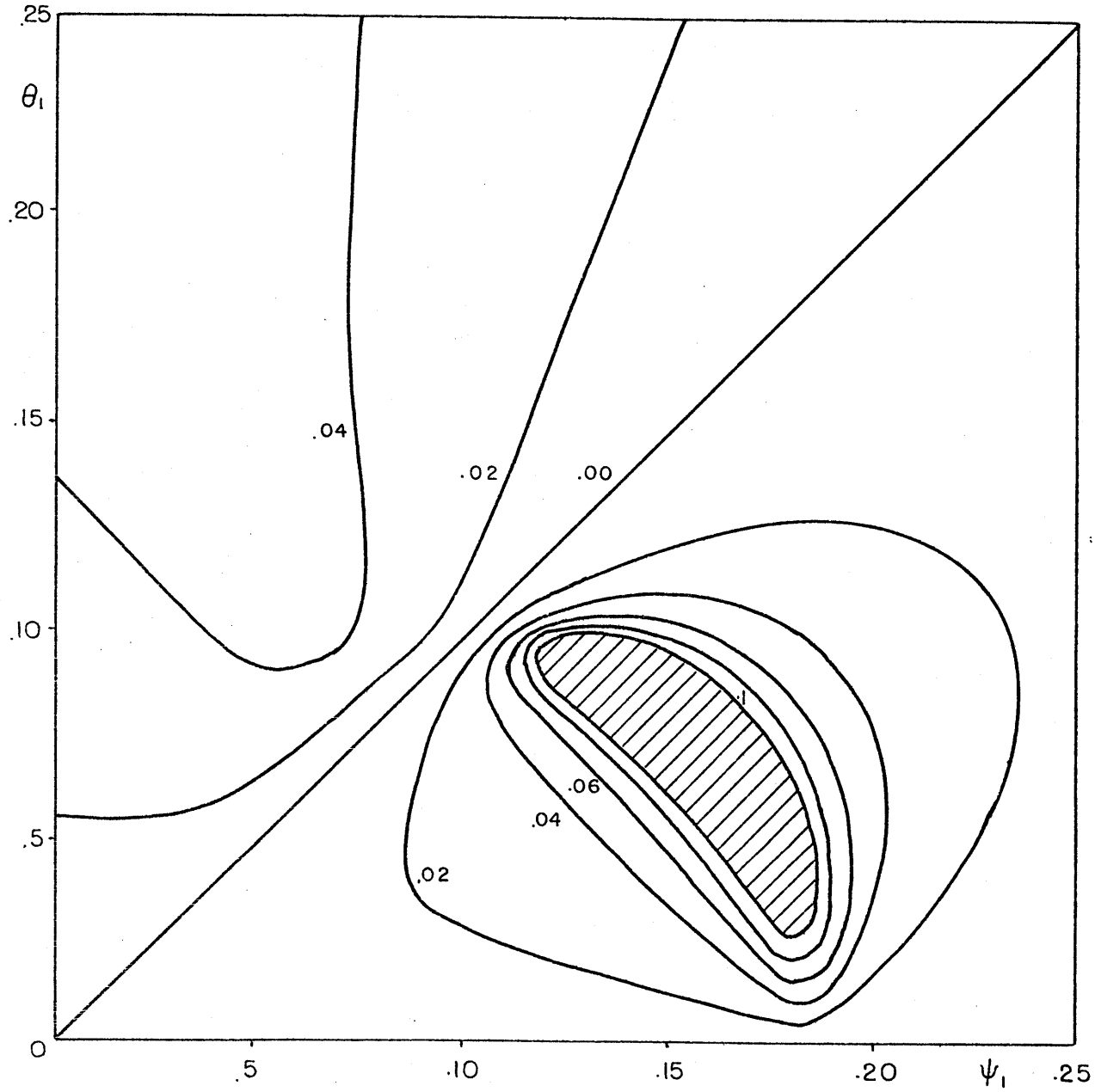

FIG. 3a

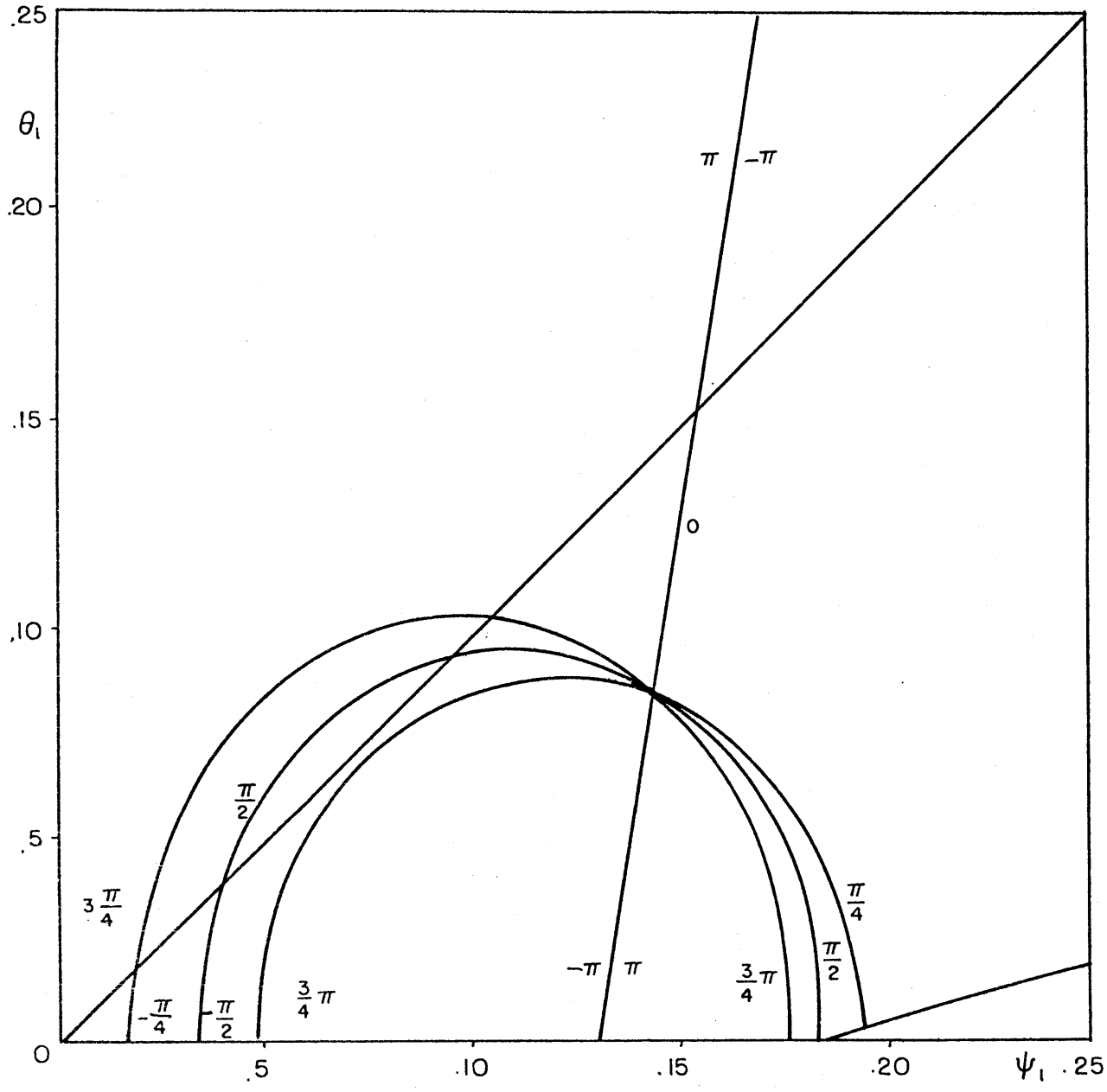
.25
θ_1
.20
.15
.10
.5
0
.5
.10
.15
.20
ψ_1 .25
π $-\pi$
0
$\frac{\pi}{2}$
$3\frac{\pi}{4}$
$\frac{\pi}{4}$
$\frac{\pi}{2}$
$-\frac{\pi}{4}$
$\frac{3}{4}\pi$
$-\pi$ π
$\frac{3}{4}\pi$
$\frac{\pi}{4}$
$\frac{\pi}{2}$

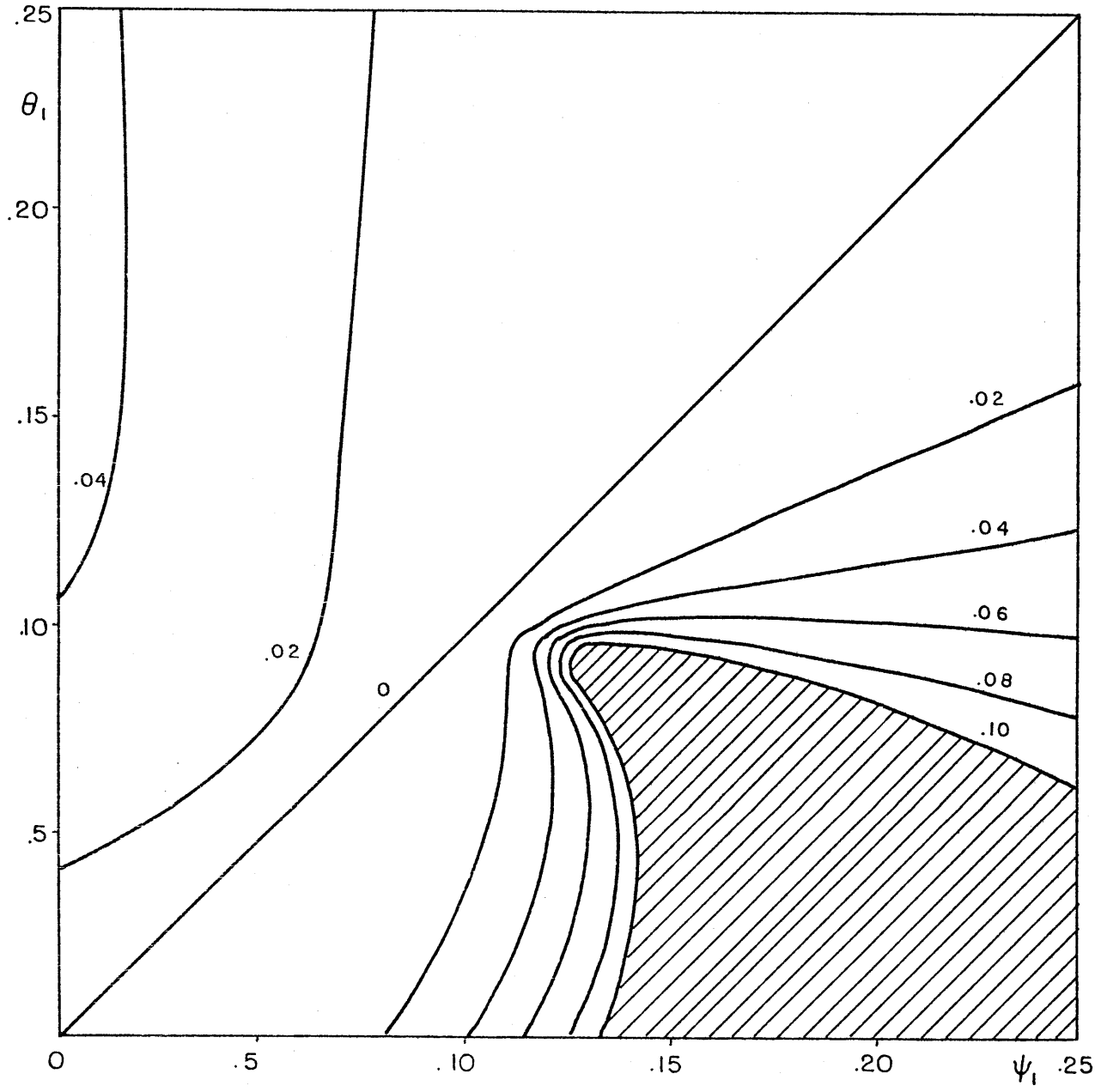
.25
θ_1
.20
.15
.10
.5
0
.5
.10
.15
.20
ψ_1 .25
.04
.02
0
.02
.04
.06
.08
.10

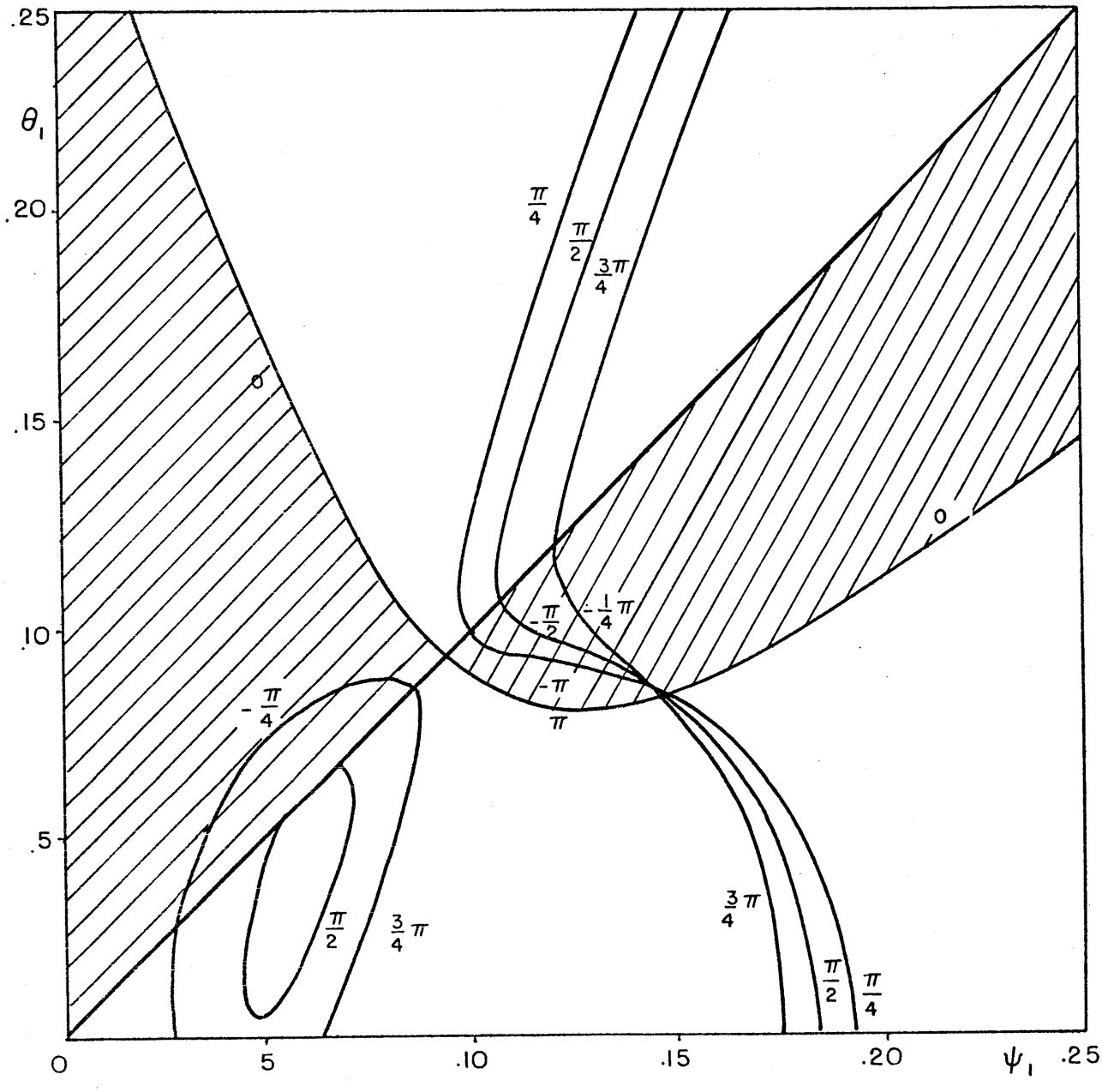
.25
θ_1
.20
.15
.10
.5
0
5
.10
.15
.20
ψ_1
.25
$\frac{\pi}{4}$
$\frac{\pi}{2}$
$\frac{3}{4}\pi$
0
$-\frac{\pi}{2}$
$-\frac{1}{4}\pi$
$-\pi$
π
$-\frac{\pi}{4}$
$\frac{\pi}{2}$
$\frac{3}{4}\pi$
$\frac{3}{4}\pi$
$\frac{\pi}{2}$
$\frac{\pi}{4}$
0

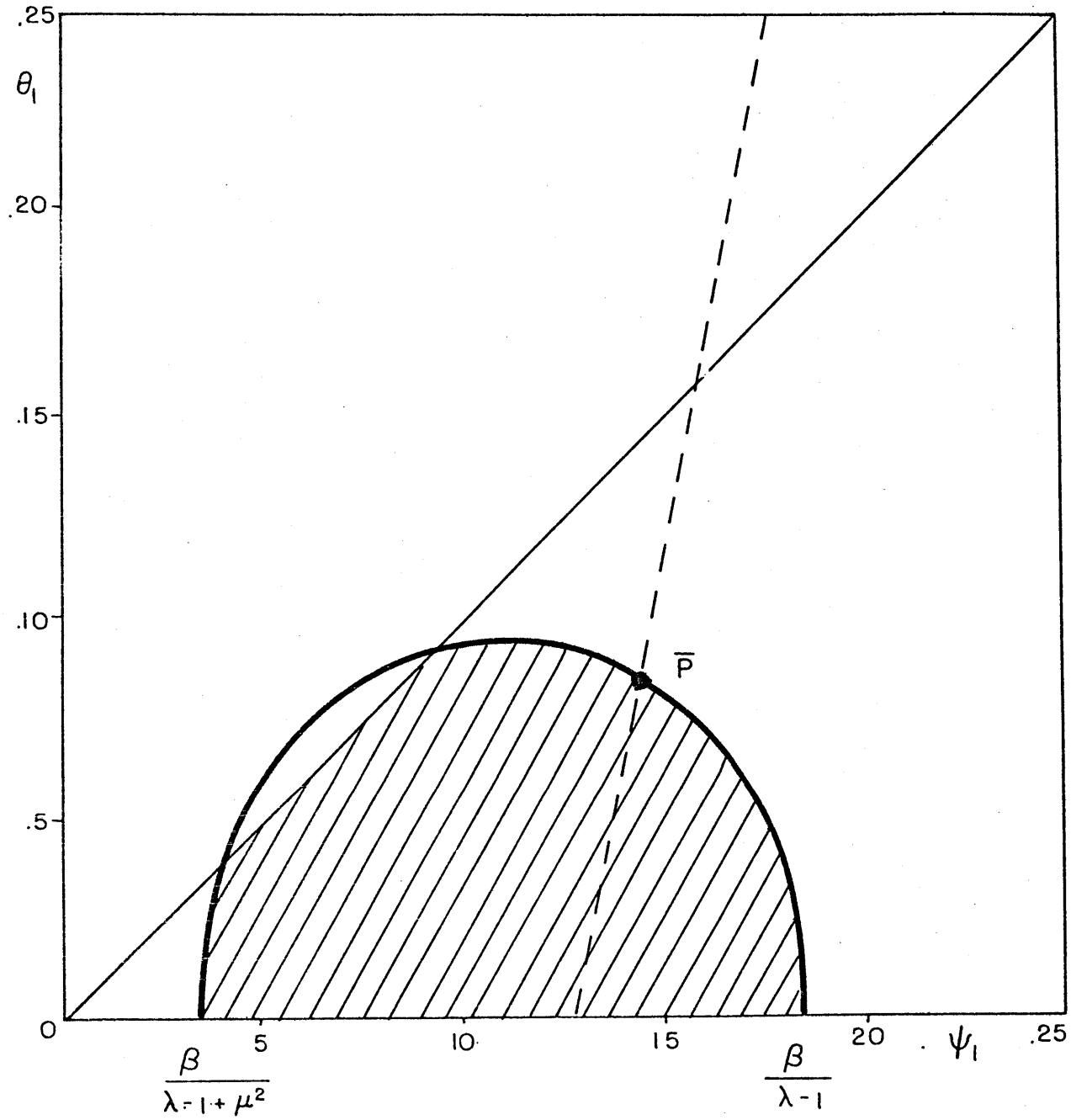
.25
θ_1
.20
.15
.10
.5
0
$\overline{P}$
5
10
15
20
.25
ψ_1
$\frac{\beta}{\lambda-1+\mu^2}$
$\frac{\beta}{\lambda-1}$

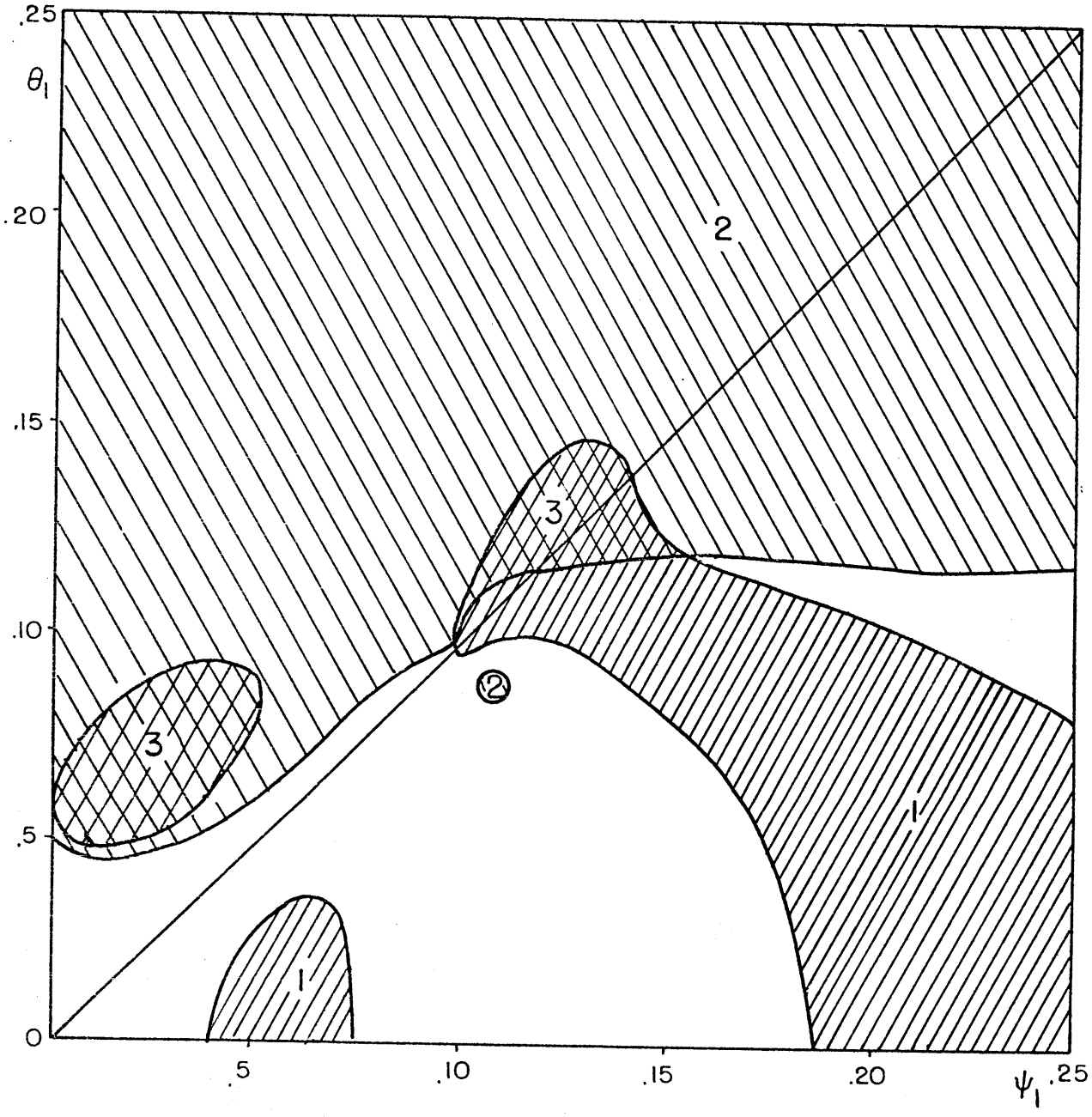
.25
θ_1
.20
.15
.10
.5
0
.5
.10
.15
.20
.25
ψ_1
1
2
3
3
1
2

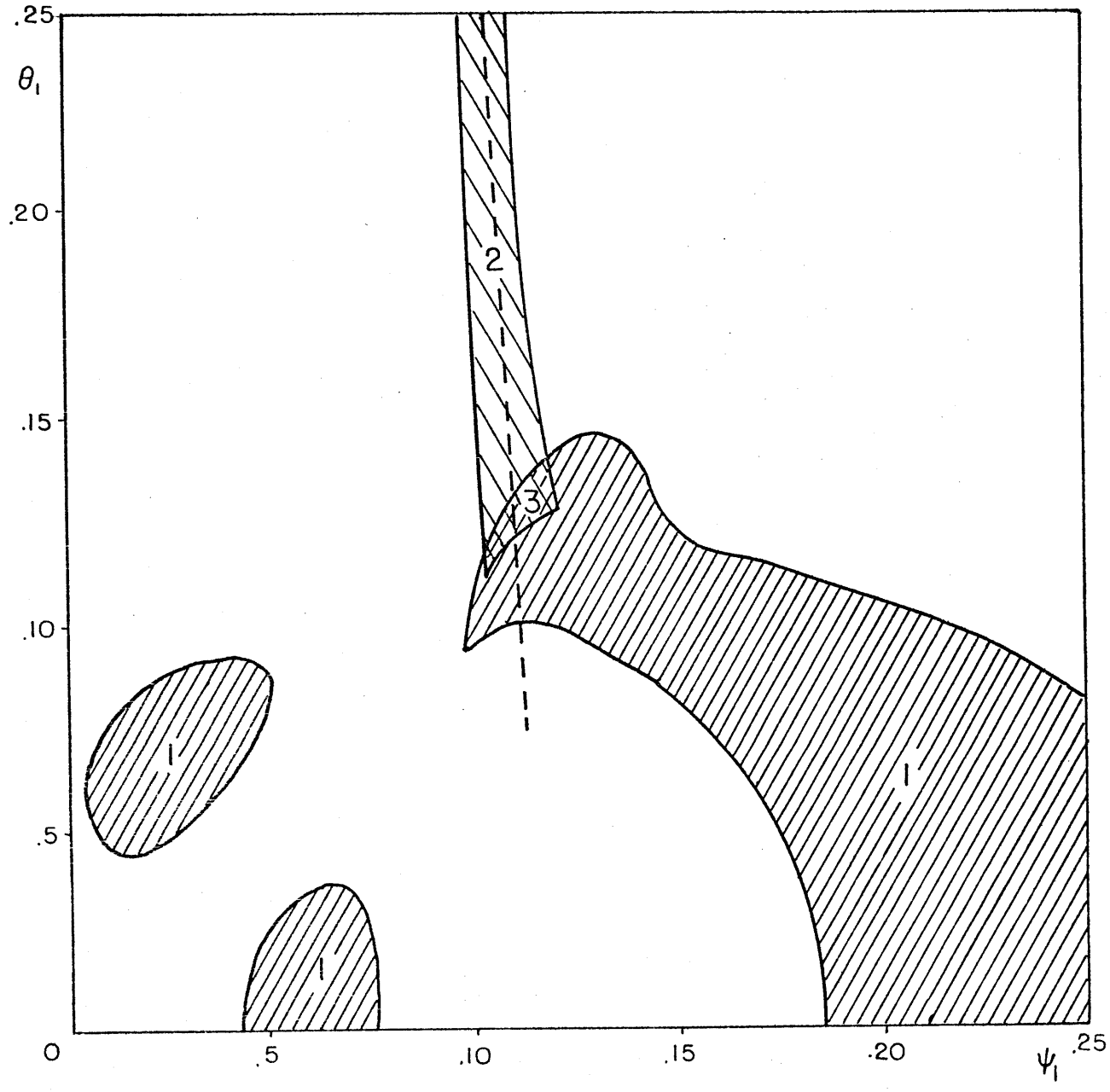
.25
θ_1
.20
.15
.10
.5
0
.5
.10
.15
.20
.25
ψ_1
1
2
3
1
1
1

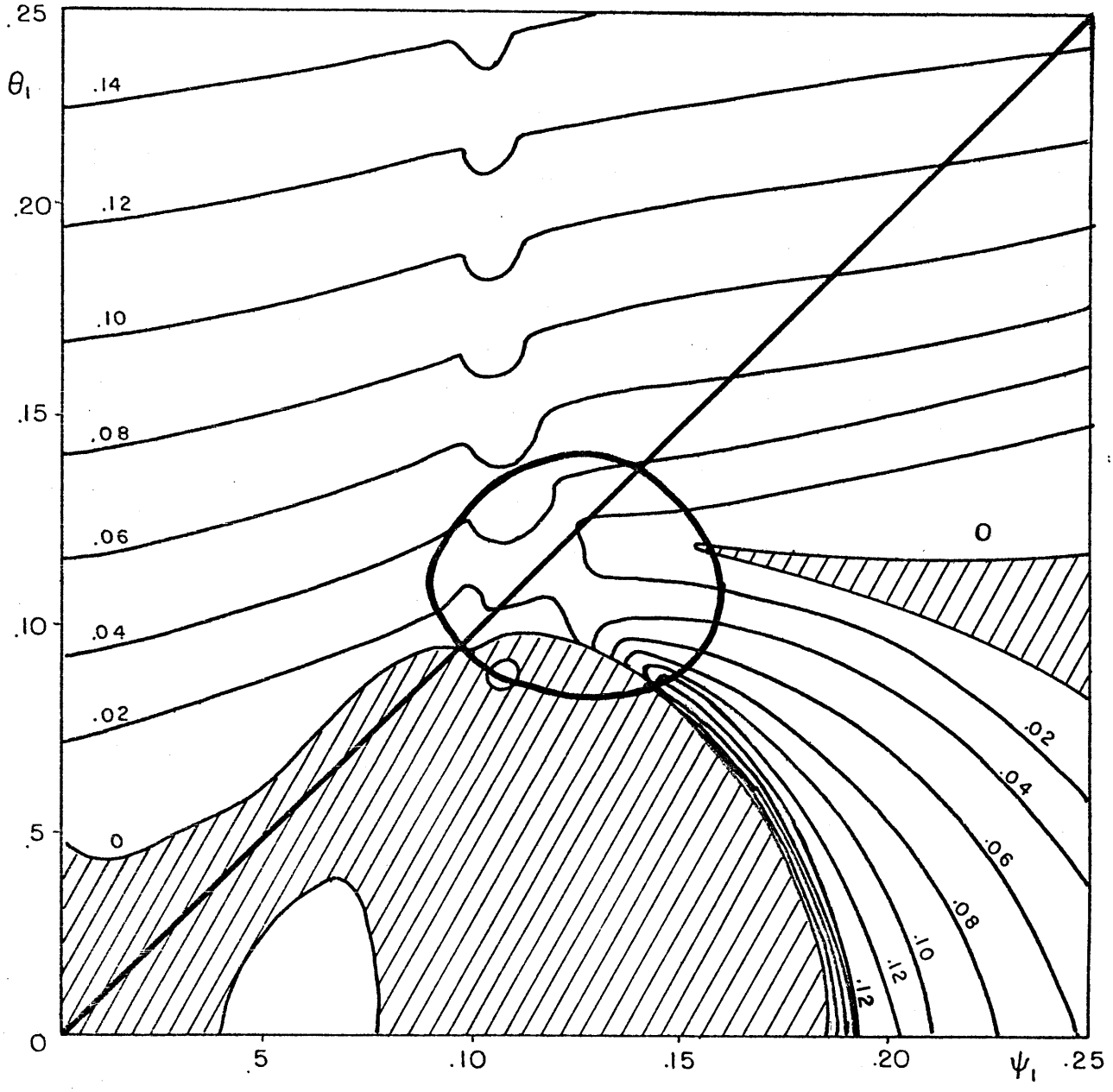
.25
θ_1
.20
.15
.10
.5
0
.14
.12
.10
.08
.06
.04
.02
0
0
.02
.04
.06
.08
.10
.12
.12
.5
.10
.15
.20
ψ_1
.25

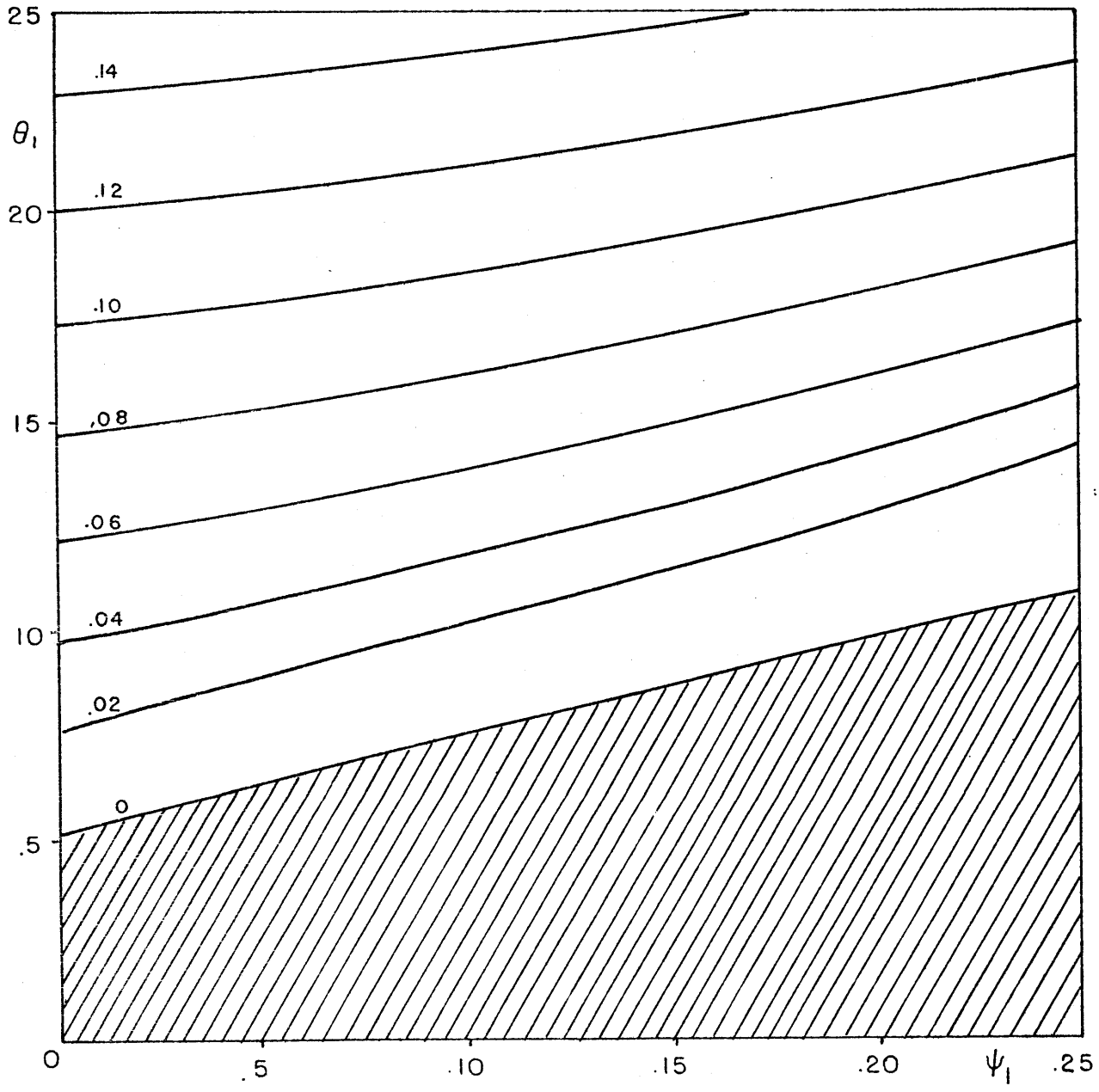
25
20
15
10
.5
0
θ_1
.14
.12
.10
.08
.06
.04
.02
0
.5
.10
.15
.20
ψ_1
.25

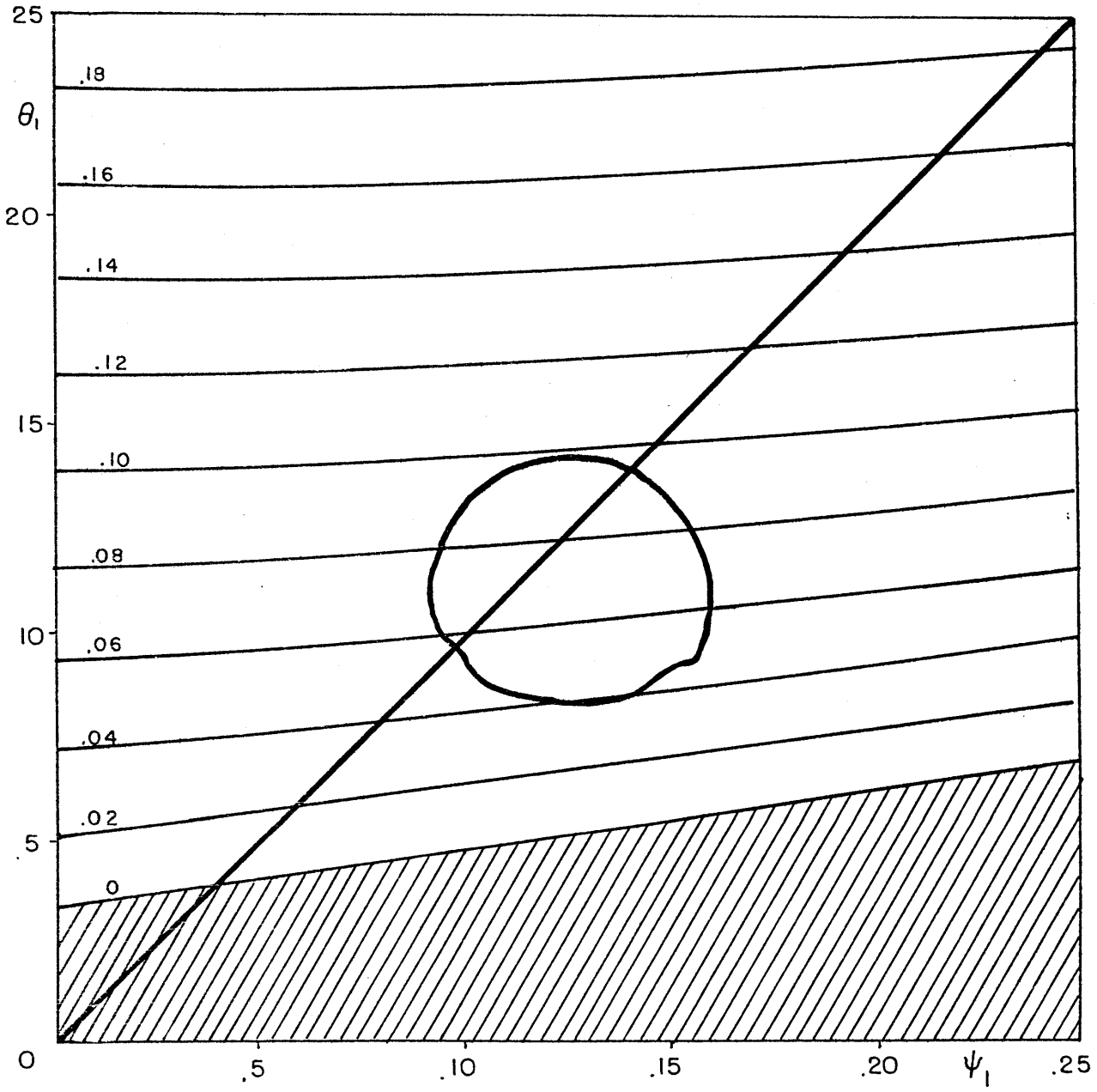
25
20
15
10
5
0
θ_1
.18
.16
.14
.12
.10
.08
.06
.04
.02
0
.5
.10
.15
.20
ψ_1
.25

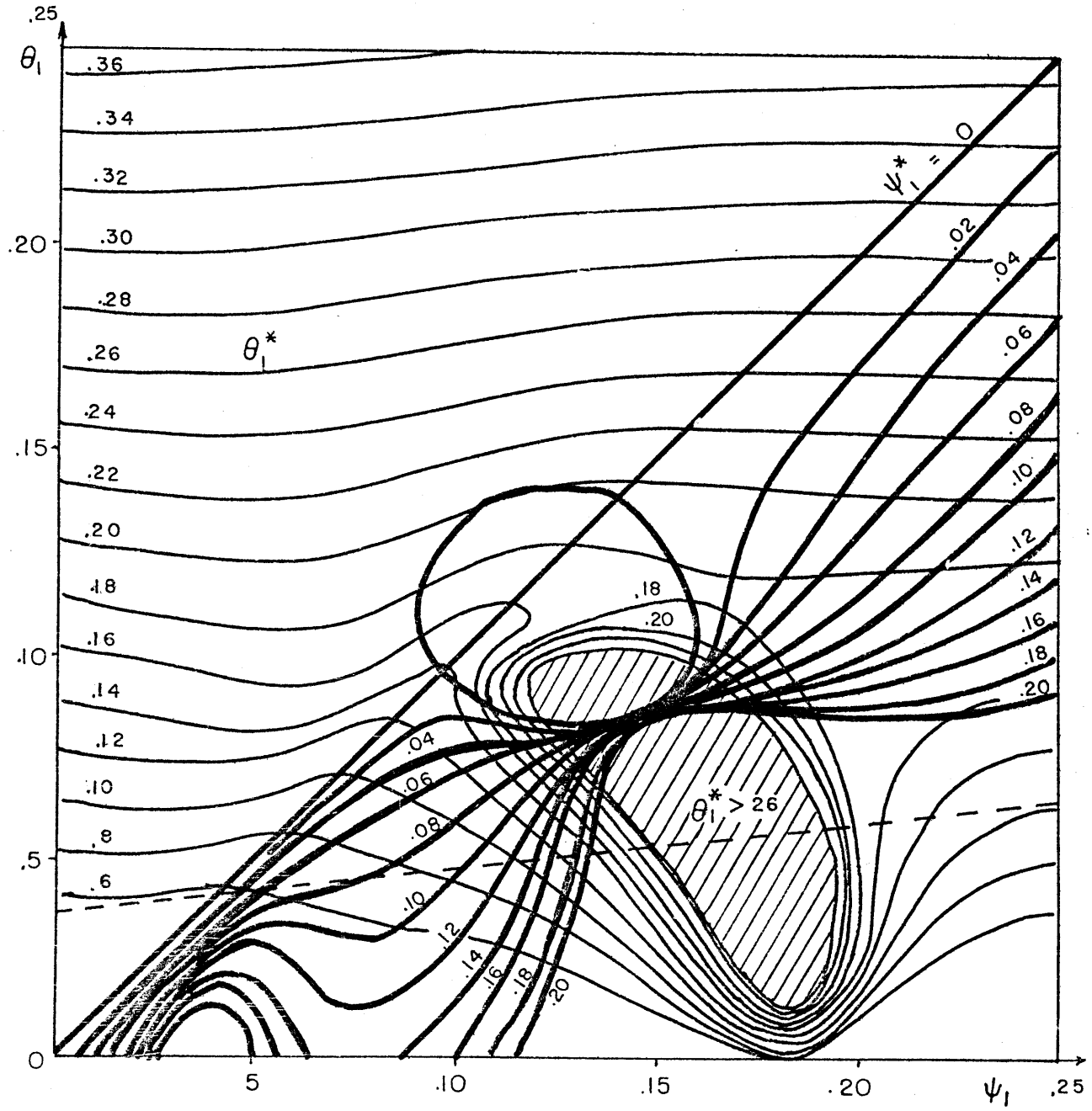
.25
θ_1
.36
.34
.32
.30
.20
.28
.26
θ_1^*
.24
.15
.22
.20
.18
.16
.10
.14
.12
.10
.8
.5
.6
0
5
.10
.15
.20
ψ_1
.25
$\psi_1^* = 0$
.02
.04
.06
.08
.10
.12
.14
.16
.18
.20
.18
.20
.04
.06
.08
.10
.12
.14
.16
.18
.20
$\theta_1^* > 26$

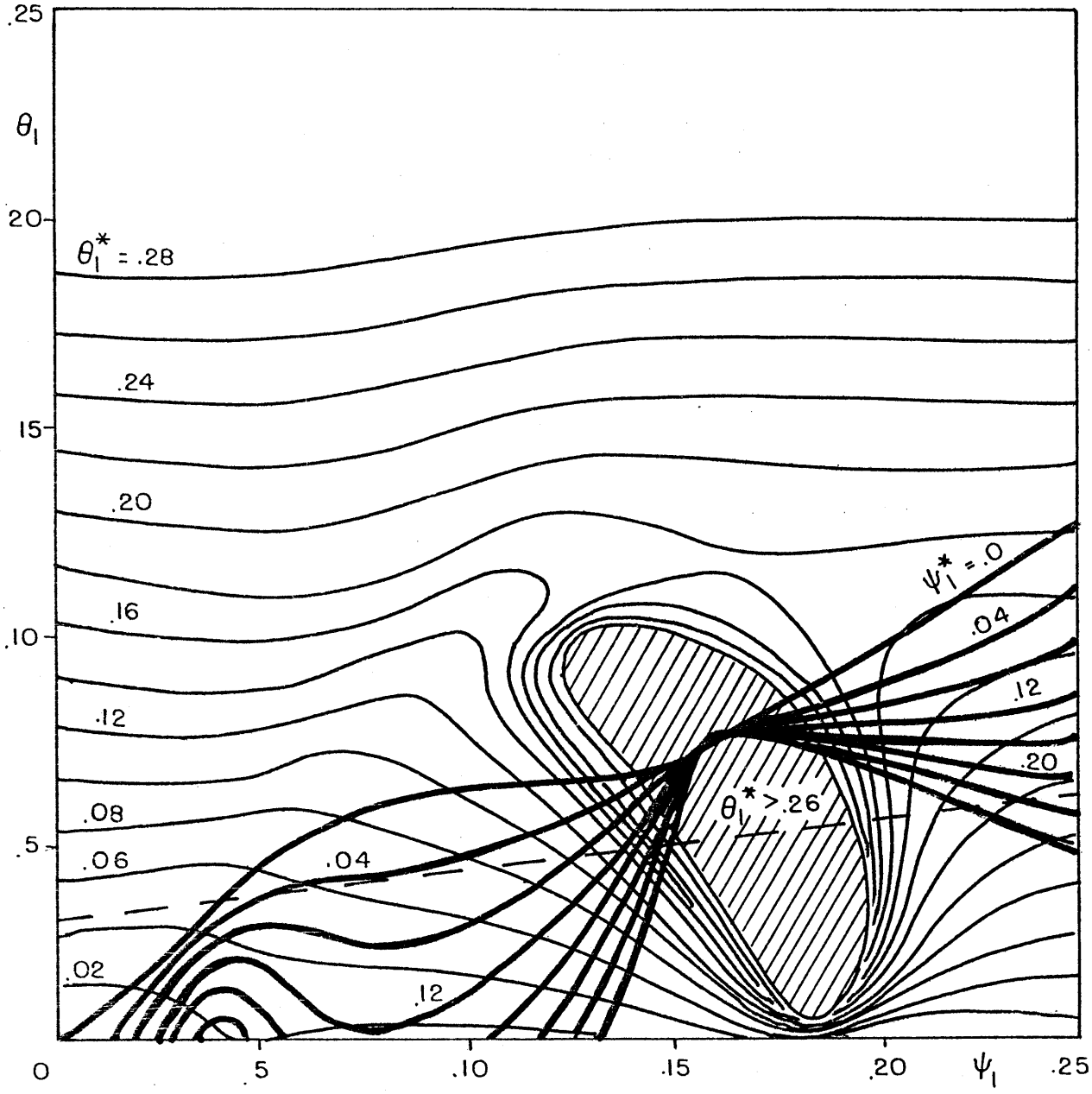
.25
θ_1
.20
$\theta_1^* = .28$
.24
.15
.20
.16
.10
.12
.08
.5
.06
.04
.02
.12
$\psi_1^* = .0$
.04
.12
.20
$\theta_1^* > .26$
0
.5
.10
.15
.20
ψ_1
.25

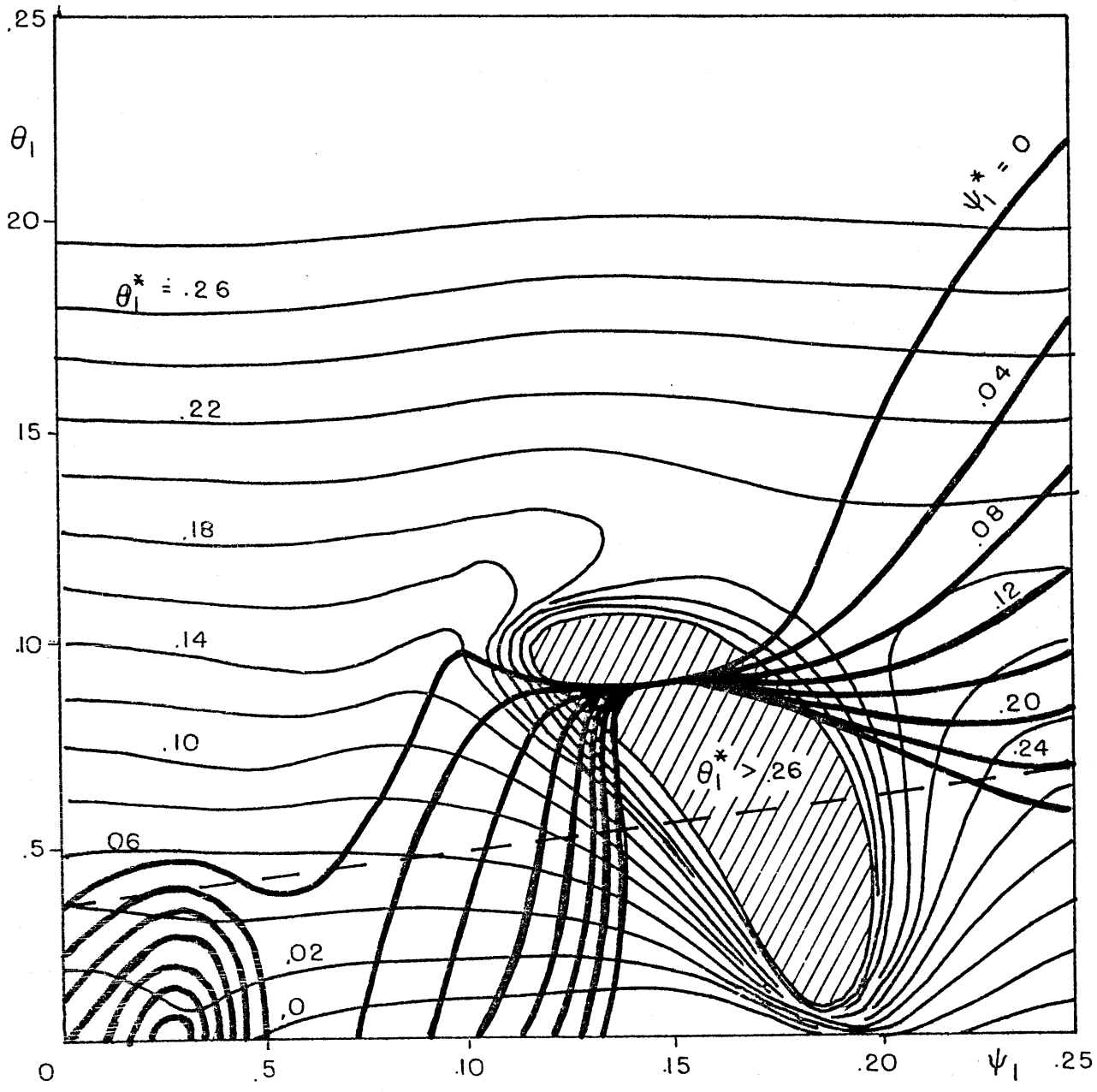
.25
θ_1
20
15
.10
.5
0
.5
.10
.15
.20
ψ_1
.25
$\theta_1^* = .26$
.22
.18
.14
.10
06
.02
.0
$\psi_1^* = 0$
.04
.08
.12
.20
.24
$\theta_1^* > .26$

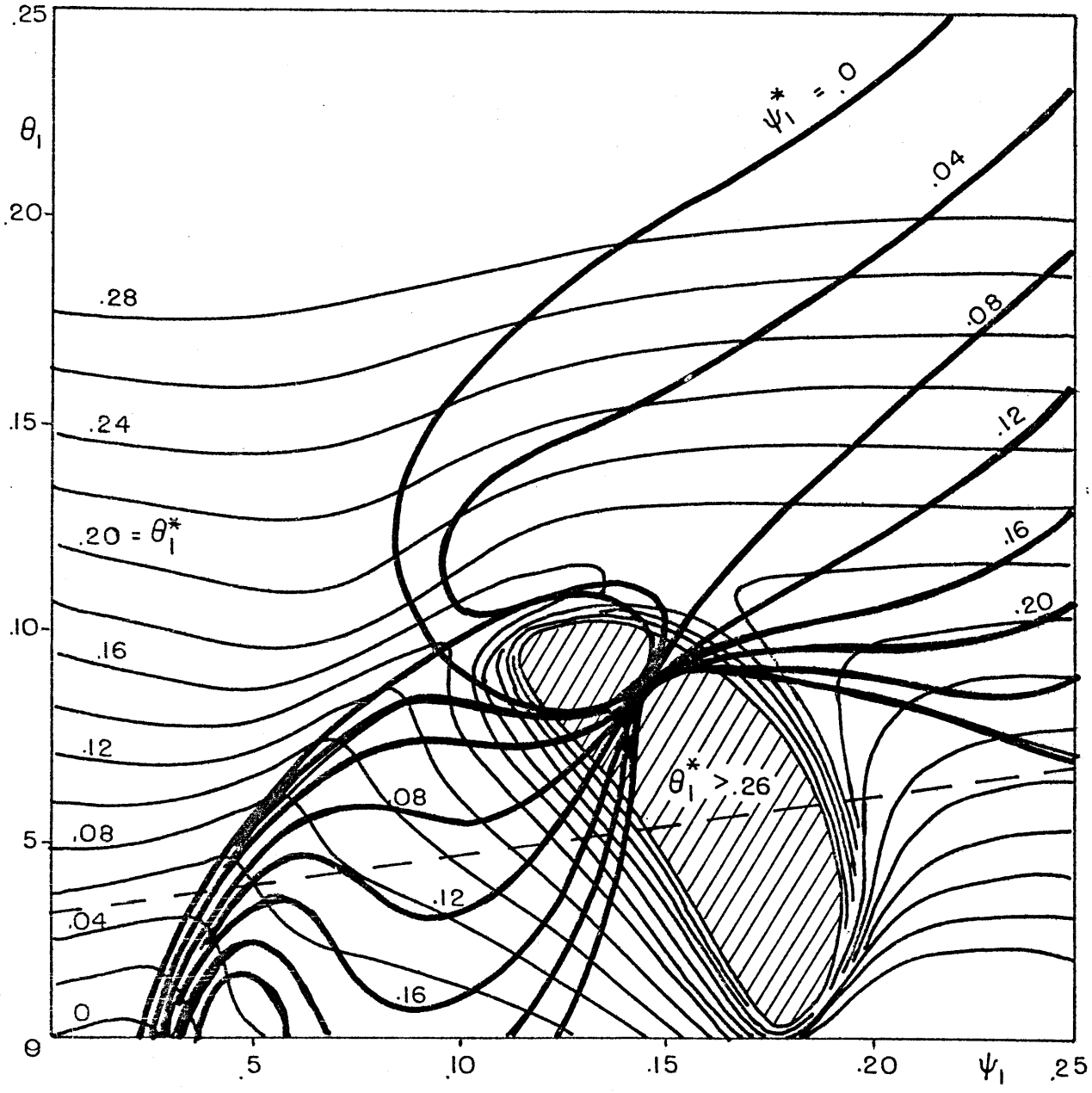
.25
θ_1
.20
.15
.10
5
0
.5
.10
.15
.20
ψ_1
.25
$\psi_1^* = .0$
.04
.08
.12
.16
.20
.28
.24
$.20 = \theta_1^*$
.16
.12
.08
.04
0
$\theta_1^* > .26$

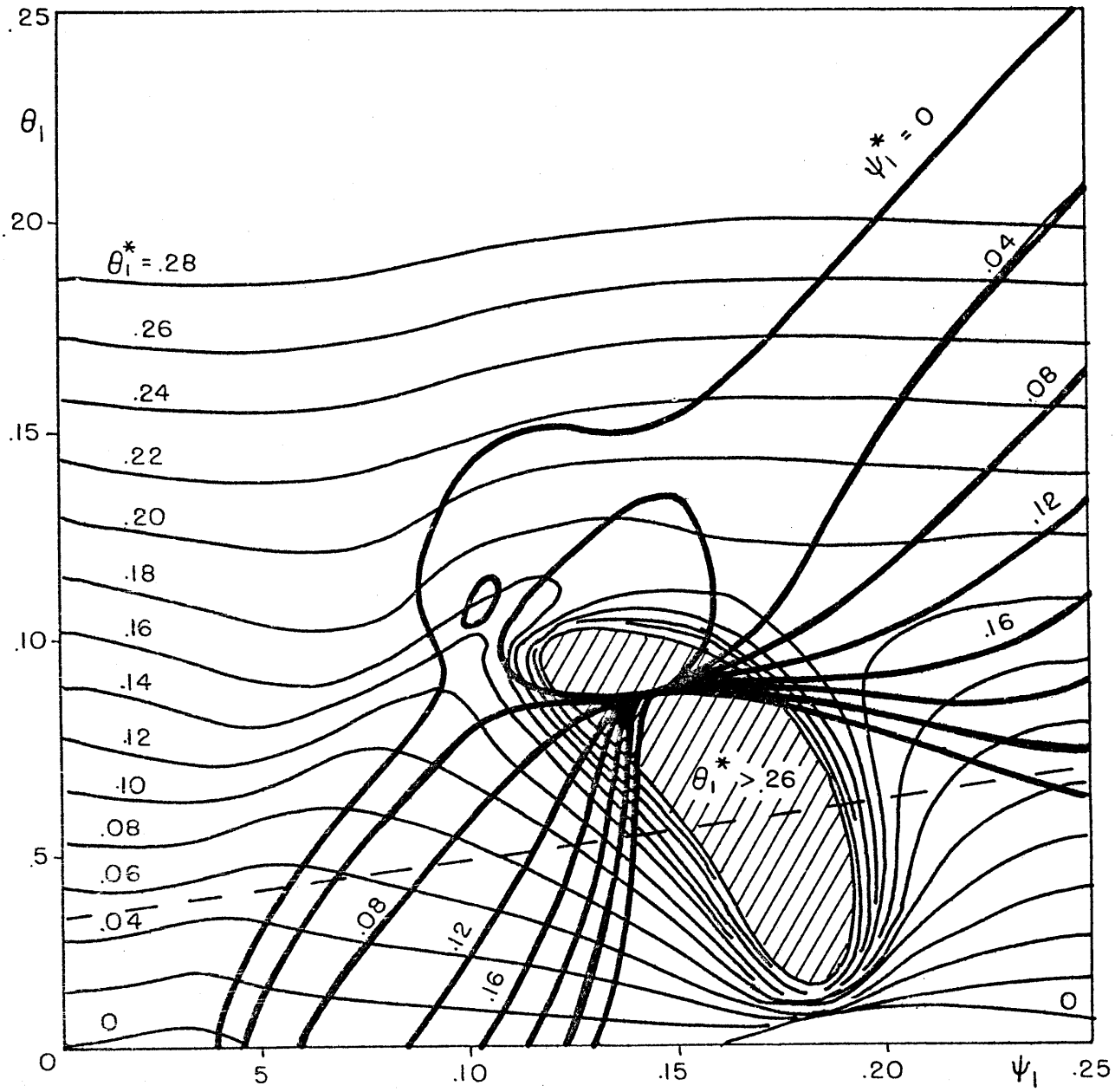
.25
θ_1
.20
.15
.10
.5
0
$\theta_1^* = .28$
.26
.24
.22
.20
.18
.16
.14
.12
.10
.08
.06
.04
0
$\psi_1^* = 0$
.04
.08
.12
.16
$\theta_1^* > .26$
.08
.12
.16
0
5
.10
.15
.20
ψ_1
.25

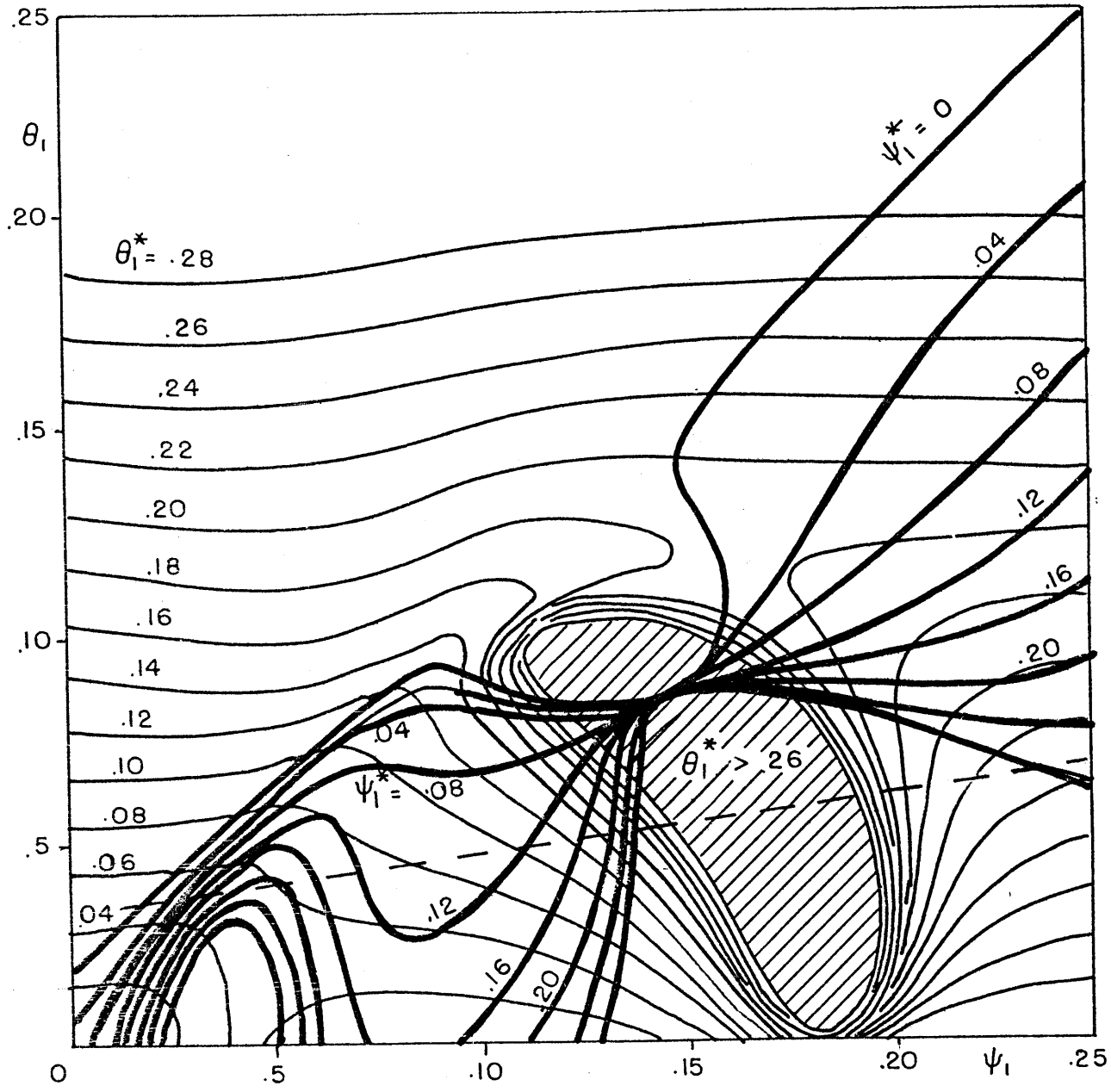
.25
θ_1
.20
.15
.10
.5
0
.5
.10
.15
.20
ψ_1
.25
$\theta_1^* = .28$
.26
.24
.22
.20
.18
.16
.14
.12
.10
.08
.06
.04
$\psi_1^* = 0$
.04
.08
.12
.16
.20
$\psi_1^* = .08$
$\theta_1^* > .26$

		Winter	Summer
Eddy fluxes of barotropic angular momentum (m^2/s^2) : BR	at 30°	16.4	7.4
	at 60°	-3.6	-1.2
Eddy convergence of barotropic angular momentum between 30° and 60° N. (m/s^2) $\frac{1}{a\cos\varphi}\frac{\partial}{\partial\varphi}$ BR		$8.5*10^{-6}$	$3.6*10^{-6}$
F_ψ^* (non-dimensional units)		$.53*10^{-3}$	$.23*10^{-3}$
Eddy fluxes of baroclinic angular momentum (m^2/s^2) : BC	at 30°	7.0	4.2
	at 60°	-1.9	-0.7
Eddy convergence of baroclinic angular momentum between 30° and 60° N. (m/s^2) $\frac{1}{a\cos\varphi}\frac{\partial}{\partial\varphi}$ BC		$3.8*10^{-6}$	$2.1*10^{-6}$
F_θ^* (non-dimensional units)		$.24*10^{-3}$	$.13*10^{-3}$

TABLE 1

SECTION 3

STATIONARY ADIABATIC FRICTIONLESS FLOW OVER TOPOGRAPHY

1. Introduction

In this last section we shall examine a stationary quasi-geostrophic inviscid flow over topography and the vertical propagation of zonal momentum and energy; we then analyze in some detail how these transports are accomplished in a simple fully non-linear solution. In particular we shall consider the implication of a top radiation boundary condition on the mean meridional circulation.

Our study clarifies the role of the stationary waves in forcing a mean meridional circulation and in particular suggests that there will be a strong meridional mass flux in the layer containing the topography. It also points out the necessity of studying the time dependent problem to increase our understanding of the mean meridional circulation in the upper atmosphere.

2. Equations of motion

We study a quasi-geostrophic adiabatic frictionless flow in a zonally periodic beta channel. We assume the validity of the hydrostatic balance and we choose to work in pressure coordinates.

We consider the following quasi-geostrophic equations:

zonal momentum equation

$$\frac{\partial u}{\partial t} + u\frac{\partial u}{\partial x} + v\frac{\partial u}{\partial y} - (f_o+\beta y)v - f_o v' = -\frac{\partial \phi}{\partial x} \qquad (2.1)$$

vorticity equation

$$\frac{\partial \nabla^2\psi}{\partial t} + J(\psi, \nabla^2\psi + f) + f_o\frac{\partial \omega}{\partial p} = 0 \qquad (2.2)$$

thermodynamic equation

$$\frac{\partial}{\partial t}\frac{\partial \psi}{\partial p} + J\left(\psi, \frac{\partial \psi}{\partial p}\right) + f_o S\omega = 0 \qquad (2.3)$$

mass conservation equation

$$\frac{\partial \omega}{\partial p} + \frac{\partial u'}{\partial x} + \frac{\partial v'}{\partial y} = 0 \qquad (2.4)$$

and the following energy equation

$$\frac{1}{2}\frac{\partial}{\partial t}\left(\overline{|\nabla\psi|^2}^{xy} + \frac{1}{S}\overline{\left(\frac{\partial \psi}{\partial p}\right)^2}^{xy}\right) = -\frac{\partial}{\partial p}\left(f_0 \overline{\omega\psi}^{xy}\right) \qquad (2.5)$$

which can be obtained by multiplying (2.2) by ψ, (2.3) by $\frac{1}{S}\frac{\partial \psi}{\partial p}$, adding them together and averaging over a p-surface.

where u eastward component of the geostrophic wind

v northward component of the geostrophic wind

u' eastward component of the ageostrophic wind

v' northward component of the ageostrophic wind

f Coriolis parameter = $2\Omega \sin\varphi \sim f_0 + \beta y$

f_0 Coriolis parameter evaluated at mid-latitude

β derivative of the Coriolis parameter = $\frac{df}{dy}$

ϕ geopotential

ψ stream-function for the geostrophic wind

∇ horizontal divergence or gradient

ω individual pressure change = $\frac{dp}{dt}$

S dry static stability = $-\frac{\alpha}{f_o^2}\frac{1}{\theta}\frac{d\theta}{dp}$

$\overline{(\ )}^{x}$ zonal average at constant p and y

$\overline{(\ )}^{xy}$ horizontal average at constant pressure

3. Simple theorems

We now proceed to prove three statements.

Theorem 1. For a stationary channel flow the total upward flux of energy, $f_0 \overline{\omega\psi}^{xy}$, must vanish.

Proof. This is a straightforward consequence of the thermodynamic equation. In fact, multiplying (2.3) by ψ and horizontally averaging, we have:

$$f_0 S \overline{\omega\psi}^{xy} = -\overline{\psi J\left(\psi, \frac{\partial\psi}{\partial p}\right)}^{xy} = -\overline{J\left(\psi, \psi\frac{\partial\psi}{\partial p}\right)}^{xy} = 0 \qquad (3.1)$$

where we have used the zonal periodicity and the presence of lateral meridional walls.

Lemma 1. If we have a stationary wave that propagates energy upward we must have a mean meridional circulation that transports back the same amount of energy.

Lemma 2. No level can be a net source of energy.

Theorem 2. For a stationary channel flow the form drag due to the topography must be balanced by the Coriolis force in the layer containing the topography.

Proof. We start from the zonal momentum equation (2.1),

and, to avoid the problem arising where p-surfaces intersect the ground, we integrate vertically from the ground (quantities evaluated at the ground are hereafter denoted with the sub-index g), $p = P_g(x,y)$, to a generic level p, then we take the spatial derivatives outside the integral to get

$$\frac{\partial}{\partial x}\int_{P_g}^{P} uu\,dp + \frac{\partial}{\partial y}\int_{P_g}^{P} uv\,dp - f\int_{P_g}^{P}(V+V')\,dp = -\frac{\partial}{\partial x}\int_{P_g}^{P}\phi\,dp - \phi_g\frac{\partial P_g}{\partial x} \qquad (3.2)$$

where the term $(u\omega)_g$ has been neglected been second order in the Rossby number. Taking a p-level, $p = P_o$ just above the topography we can perform a horizontal average. All the terms having in front a horizzontal derivative vanish due to our zonal periodicity and our meridional boundary conditions and we are left with

$$-f\overline{\int_{P_g}^{P_o}(V+V')\,dp}^{xy} = g\,\overline{P_g\frac{\partial h}{\partial x}}^{xy} \qquad (3.3)$$

Lemma 3. If the net meridional flux of mass is zero at all latitudes the form drag must vanish. In fact Eq. (3.2) is valid once p is lower than any ground pressure; in particular we can choose p = 0.

Because we are working with quasi geostrophic

equation we conclude that the form-drag must be a second order term in the Rossby number. To point out more clearly this result we can do the quasi-geostrophic scaling on the zonal momentum equation

$$\frac{\partial u}{\partial t} + \frac{\partial uu}{\partial x} + \frac{\partial uv}{\partial y} + \frac{\partial u\omega}{\partial p} - fv = -\frac{\partial \phi}{\partial x}$$

where now (U, V, ω) are the full components of the velocity field. We scale all our variables in the quasi geostrophic framework

$$\begin{aligned}
(x,y) &= L\,(x',y') \\
p &= P_0\, p' \\
t &= (L/U_0)\, t' \\
(u,v) &= U_0\,(u',v') \\
\phi &= f_0 U_0 L\, \phi' \\
\omega &= R_0 \frac{U_0 P_0}{L}\, \omega'
\end{aligned}$$

where Ro is the Rossby number $R_0 = U_0/Lf_0$, and P_0 , the typical value of the ground pressure, has been choosen to scale the vertical variations of the pressure field. Substituting we get

$$R_0\left(\frac{\partial u'}{\partial t'} + \frac{\partial u'u'}{\partial x'} + \frac{\partial u'v'}{\partial y'} + R_0\frac{\partial u'\omega'}{\partial p'}\right) - \left(\frac{f}{f_0}\right)v' = -\frac{\partial \phi'}{\partial x'}$$

Integrating from P_g' to $P'=0$ and horizontally averaging we find:

$$R_o^z \overline{u'\omega'}^{xy}(p'=0) - \frac{f}{\rho_o}\overline{\int_{P_g'}^{0} v'\,dp'}^{xy} = -\overline{\phi_g' \frac{\partial P_g'}{\partial x'}}^{xy}$$

and assuming no meridional mass flux

$$R_o^z \left(\overline{u'\omega'}^{xy}\right)_{p'=0} = -\left(\overline{\phi' \frac{\partial p'}{\partial x'}}^{xy}\right)_{p'=p_g'}$$

Transforming the x-derivative following the ground to x-derivative at constant height, using the definition of geostrophic wind in z-coordinates and neglecting the horizontal variations of the ground density, $\rho_g \sim \rho_o$, we can write:

$$R_o^z \left(\overline{u'\omega'}^{xy}\right)_{p'=0} = -\left(\overline{\phi' \frac{\partial p'}{\partial x}}^{xy}\right)_{p'=p_g'} \simeq -\overline{v' \frac{h}{H}}^{xy}$$

where now H is the internal height scale defined as $H = (g\rho_o/p_o)^{-1}$. Assuming a realistic small topography, $h/H \simeq Ro$, we find that the part of the meridional wind

correlated with the topography must be of order Rossby number. In the linear theory of topographically forced waves this does not hold when we go close to a resonance so that the linear theory must break down.

Our third statement is a relation between the form drag and the vertical component of the Palm and Eliassen flux.

We start by considering the zonally averaged zonal momentum equation

$$\frac{\partial \overline{u}^x}{\partial t} = -\frac{\partial \overline{uv}^x}{\partial y} + f_0 \overline{v'}^x \tag{3.4}$$

We write the ageostrophic wind using the zonally averaged continuity and thermodynamic equations

$$\frac{\partial \overline{v'}^x}{\partial y} = -\frac{\partial \overline{\omega}^x}{\partial p} = \frac{\partial}{\partial p} \frac{1}{f_0 S} \overline{J\left(\psi, \frac{\partial \psi}{\partial p}\right)}^x$$

$$\frac{\partial}{\partial y}\left(\overline{v'}^x - \frac{\partial}{\partial p} \frac{1}{f_0 S} \overline{v \psi_p}^x\right) = 0$$

We integrate once in y, using the meridional boundary condition, $\overline{v} = \overline{v'} = 0$ on the lateral boundary, to get

$$\overline{v'}^x = \frac{\partial}{\partial p} \frac{1}{f_0 S} \overline{v \psi_p}^x \tag{3.5}$$

We then substitute $\overline{v'}^{x}$ in (3.4) getting

$$\frac{\partial \overline{u}^{x}}{\partial t} = -\frac{\partial \overline{uv}^{x}}{\partial y} - \frac{\partial}{\partial p}\left(-\frac{1}{S}\overline{v\frac{\partial \psi}{\partial p}}^{x}\right) \qquad (3.6)$$

where now on the right hand side we have the divergence of the Palm and Eliassen flux (Andrew and McIntyre, 1976). The second term on the R.H.S can be interpreted as a vertical convergence of "geostrophic vertical flux of zonal momentum."

Theorem 3. For a stationary flow the total "geostrophic vertical flux of zonal momentum" is constant with pressure and it is related to the topography by:

$$-\frac{1}{S}\overline{v\frac{\partial \psi}{\partial p}}^{xy} = \overline{\left(1-\frac{\beta}{f_0}y\right) g P_g \frac{\partial h}{\partial x}}^{xy} \qquad (3.7)$$

Proof. We consider the zonal averaged thermodynamic equation

$$\overline{\omega}^{x} = -\frac{\partial}{\partial y}\left(\frac{1}{f_0 S}\overline{v\frac{\partial \psi}{\partial p}}^{x}\right)$$

on a pressure surface P above the topography, then we vertically integrate the conservation of mass from $P_g(x,y)$

to P_0 and we zonally average to get:

$$\overline{\omega}^{x} = -\frac{\partial}{\partial y}\overline{\int_{P_4}^{P_0}(v+v')\,dp}^{x}$$

Equating these two expressions for $\overline{\omega}^{x}$ and integrating once in the meridional direction we get:

$$\frac{1}{S}\overline{v\frac{\partial\psi}{\partial p}}^{x} = f_0\overline{\int_{P_4}^{P_0}(v+v')\,dp}^{x} \qquad (3.8)$$

Using Eq. (3.3), substituting f by $f_0 - \beta y$ and neglecting second-order terms in the Rossby number, we can rewrite the R.H.S of Eq. (3.8) as

$$\frac{1}{S}\overline{v\frac{\partial\psi}{\partial p}}^{xy} = f_0\overline{\int_{P_4}^{P_0}(v+v')\,dp}^{xy} = -\beta y\overline{\int_{P_4}^{P_0}v\,dp}^{xy} - g\overline{P_4\frac{\partial h}{\partial x}}^{xy}$$

substituting the definition of geostrophic streamfunction, taking the partial x-derivative outside the integral sign and integrating once by part we find:

$$\frac{1}{S}\overline{v\frac{\partial\psi}{\partial p}}^{xy} = \frac{\beta}{f_0}g\,\overline{y\,P_4\frac{\partial h}{\partial x}}^{xy} - g\overline{P_4\frac{\partial h}{\partial x}}^{xy}$$

proving the theorem.

Lemma 4. For small topography

$$-\frac{1}{S}\overline{v\psi_p}^{x} = g\,\overline{P_g\frac{\partial h}{\partial x}}^{x} \qquad (3.9)$$

This result, without any y-integration, comes from (3.8) if we neglect the coupling between the ageostrophic wind and the topography; i.e., we neglect $\int_{P_g}^{P_o} v'\,d\rho$.

4. A simple non-linear analytical solution

We now solve a particular case and we study how these requirements are satisfied.

We use the quasi-geostrophic potential vorticity equation, obtained by eliminating ω between (2.2) and (2.3),

$$J\left(\psi, \nabla^2\psi + \beta y + \frac{\partial}{\partial p}\frac{1}{S}\frac{\partial}{\partial p}\psi\right) = 0 \qquad (4.1)$$

To define the bottom boundary condition we consider that the ground is a material surface:

$$\frac{d}{dt}\left(p - p_g\right) = \omega - \vec{v}\cdot\nabla p_g = 0$$

Where in the stationary case the ground pressure is only a function of x and y. Transforming the horizontal derivatives following the ground to horizontal derivatives at constant height, and using the hydrostatic balance, we can write:

$$\omega = \left(\vec{v}\cdot\nabla p\right)_{z=\text{const}} - \rho_g g \vec{v}\cdot\nabla h \simeq -\rho_g g \vec{v}\cdot\nabla h \qquad (4.2)$$

In the last expression we have neglected the advection of the ageostrophic pressure, which is a second order term.

We approximate this boundary condition assuming a small topography and consistently we assume a constant ground density ρ_0 and we apply (4.2) on a constant pressure level P_0, instead that on $p = P_g$.

Eliminating ω between the thermodynamic equation (2.3) and (4.2) we get

$$J\left(\psi, \frac{\partial \psi}{\partial p} - f_0 S \rho_0 g h\right) = 0 \qquad \text{at } p = P_0 \qquad (4.3)$$

An analytical solution of (4.1) and (4.3) can be obtained assuming the quasi-geostrophic potential vorticity to be a linear function of the geostrophic stream-function

$$\nabla^2 \psi + \beta y + \frac{\partial}{\partial p} \frac{1}{S} \frac{\partial}{\partial p} \psi = \alpha \psi \qquad (4.4)$$

and assuming

$$\frac{\partial \psi}{\partial p} = f_0 S \rho_0 g h \qquad \text{at } p = P_0 \qquad (4.5)$$

Putting in explicity the barotropic zonal flow

$$\psi = -Uy + \phi \tag{4.6}$$

and setting $\alpha = -\beta/U$ we can rewrite (4.5) and (4.6) as:

$$\nabla^2\phi + \frac{\partial}{\partial p}\frac{1}{S}\frac{\partial}{\partial p}\phi + \frac{\beta}{U}\phi = 0$$

$$\frac{\partial\phi}{\partial p} = f_0 S g_0 h \qquad \text{at } p = p_0 \tag{4.7}$$

These equations are linear and can be easily solved for any assigned topography.

To solve the problem we approximate, following Wiin-Nielsen (1959), the dry static stability as:

$$S \simeq \left(\tilde{H}/p\right)^2 \qquad m^2 \cdot mb^{-2}$$

where $\tilde{H}$ at mid-latitude is approximatly $1.07 * 10^6$ m. We define the following non-dimensional quantities:

$$\begin{aligned} p &= p_0\, p' \\ (x, y) &= L\,(x', y') \\ \phi &= \phi_0 \frac{1}{\sqrt{p'}}\phi' \\ h &= H\, h' \end{aligned} \tag{4.8}$$

where πL is the meridional width of the channel, P_o is a reference ground pressure, P_o = 1000 mb, $\phi_o = f_o \tilde{H}^2$, and H is an internal scale height, $H = P_o/\rho_o g \simeq 8$ km. With these substitutions and introducing a new vertical coordinate $\varphi = -\rho_o g \rho'$ Eq. (4.7) becomes:

$$\nabla^2 \phi' + \left(\frac{L}{\tilde{H}}\right)^2 \frac{\partial^2 \phi'}{\partial \varphi^2} + \left[\frac{\beta L^2}{U} - \left(\frac{L}{2\tilde{H}}\right)^2\right]\phi' = 0$$

$$\frac{\partial \phi'}{\partial \varphi} = -\frac{1}{2}\phi' - h' \qquad (4.9)$$

Assuming no topography on the meridional walls of the channel we can use a Fourier expansion

$$h' = \Sigma_{\mu\rho} h'_{\mu\rho} \sin \rho y' \sin (k_\mu x' + \varphi_{\mu\rho})$$

Where $k_\mu = \mu \cdot \frac{2\pi L}{L_x}$ and L_x is the channel lenght. Because of the linearity of the problem we can consider each component independently. We must consider two cases, for

$$\left[\frac{\beta L^2}{U} - \left(\frac{L}{2\tilde{H}}\right)^2\right] - (k_\mu^2 + \rho^2) = -\left(\frac{L}{\tilde{H}}\right)^2 \eta^2 < 0$$

the forced wave decays exponentially and the solution is given by:

$$\phi'_{\mu\rho} = e^{-\eta\varphi}\left\{A\sin(k_\mu x' + \varphi_{\mu\rho}) + A'\cos(k_\mu x' + \varphi_{\mu\rho})\right\}\sin\rho y' \qquad (4.10)$$

and applying the bottom boundary condition we get

$$A = \frac{h'_{\mu\rho}}{\eta - \frac{1}{2}} \qquad A' = 0 \qquad (4.11)$$

We see that the forced wave is in phase with the topography and therefore the form drag vanishes. In the second case,

$$\left[\frac{\beta L^2}{U} - \left(\frac{L}{2\tilde{H}}\right)^2\right] - \left(k_\mu^2 + \rho^2\right) = \left(\frac{L}{\tilde{H}}\right)^2 m^2 > 0$$

the solution has upward, A and A', and downward, B and B', energy propagating waves and it is given by:

$$\phi'_{\mu\rho} = \sin\rho y'\left\{A\sin(k_\mu x' + m\varphi + \varphi_{\mu\rho}) + A'\cos(k_\mu x' + m\varphi + \varphi_{\mu\rho})\right.$$
$$\left. + B\sin(k_\mu x' - m\varphi + \varphi_{\mu\rho}) + B'\cos(k_\mu x' - m\varphi + \varphi_{\mu\rho})\right\} \qquad (4.12)$$

and applying the bottom boundary condition we get

$$m(A - B) = -\frac{1}{2}(A' + B')$$

$$m(A' - B') = \frac{1}{2}(A + B) + h'_{\mu\rho}$$

Applying a top radiation boundary condition to determine the solution we have:

$$B = B' = 0$$

$$A = -\frac{2 h_{\mu\rho}}{1+4\mu^2} \qquad A' = -2\mu A \tag{4.13}$$

Because the solution is not in phase with the topography we now have a topographic form drag. To get no form drag and to satisfy the bottom boundary condition we must have

$$A' = B' = 0 \qquad A = B = -h'_{\mu\rho}$$

i.e., we have two waves with the same amplitude, one propagating upward and the other downward.

The most interesting solution is that obtained with the top radiation boundary condition because it does not require a source of wave energy at infinity; in presence of a single-mode topography this is given by

$$\psi = -UL y' - \phi_0 \frac{2 h'_{\mu\rho}}{1+4\mu^2} \left\{ \sin(k_\mu x' + \mu\varphi) + \right. \tag{4.14}$$

$$\left. - 2\mu \cos(k_\mu x' + \mu\varphi) \right\}$$

As we have said, this solution transfers wave energy upward; hence, for Theorem 1, we must have a mean meridional circulation that transfer energy downward. The vertical energy flux due to the mean meridional circulation is given by $f_0 \overline{\omega^x \psi^x}^y = -f_0 UL \overline{\omega^x}^y$

The vertical motion can be computed from the thermodynamic equation (2.3)

$$f_0 \omega = \frac{1}{S} J\left(\psi, \frac{\partial \psi}{\partial p}\right) =$$

(4.15)

$$= -\left(\frac{P_0}{\tilde{H}}\right)^2 \frac{1}{P_0} \left\{ \sqrt{\rho'} \phi_0 U \frac{\partial}{\partial x} \left(\phi'_\varphi + \frac{1}{2}\phi'\right) + \phi_0^2 J\left(\phi', \frac{\partial \phi'}{\partial \varphi}\right) \right\}$$

and the zonal average $\overline{\omega}^x$ reduces to

$$\overline{\omega}^x = -f_0 P_0 \left(\frac{\tilde{H}}{L}\right)^2 \frac{\partial}{\partial y'} \overline{\frac{\partial \phi'}{\partial x'} \frac{\partial \phi'}{\partial \varphi'}}^x =$$

(4.16)

$$= -f_0 P_0 \left(\frac{\tilde{H}}{L}\right)^2 k_4 m \rho \frac{2h'^2}{1+4m^2} \sin 2\rho y'$$

independent of the pressure. Hence, due to the mean meridional motion we have a downward flux of energy, independent of height, that balances exactly the upward flux of wave energy. To understand the source of this energy at infinity we should consider the time dependent problem and

study the upward propagation of the wave front; the mean meridional circulation should be set up behind the wave front that should be also the source of the energy which is advected downward.

From Eq. (4.16) we also see that at some latitudes we get a constant upward mass flux starting from the surface $p = P_o$ and leaving the atmosphere while at other latitudes we get a mass flux entering the upper atmosphere and coming down to the surface $p = P_o$. From Theorem 2 we can anticipate that in the layer containing the topography there will be a net meridional transfer of mass able to close the lower part of the meridional circulation. To close the upper part of the mean meridional circulation we think that we should, as we said before, study the time evolution of the wave front.

REFERENCES

Andrews, D.G., and M.E. McIntyre, 1976: Planetary waves in horizzontal and vertical shear: the generalized Eliassen-Palm relation and the mean zonal acceleration. J. Atmos. Sci., 33, 2031-2048

Wiin-Nielsen, A., 1959: On barotropic and baroclinic models, with special emphasis on ultra-long waves. Mon. Wea. Rev., 87, 171-183.